Single Shot Phase Shifting Interferometry based on Polarization Techniques

David Ignacio Serrano García

Submitted for the degree of
Doctor of Science (Optics)

León, Guanajuato, México.

March 2014

Single Shot Phase Shifting Interferometry based on Polarization Techniques

MSc. David Ignacio Serrano García
Centro de Investigaciones en Óptica A.C.

Date:_____
Approved:

_____	_____
Dr. Amalia Martínez García, Advisor	Dr. Noel Iván Toto Arellano, Co-Advisor
Centro de Investigaciones en Óptica A.C.	Universidad Tecnológica de Tulancingo
León, Gto, México.	Tulancingo, Hidalgo, México.

Thesis submitted in partial fulfillment of
the requirements for the degree of Doctor
of Science (Optics) at Centro de Investigaciones en Óptica A. C.
León, Guanajuato, México. March 2014

Abstract

Phase-shifting interferometry techniques (PSI) require several phase-shifted interferograms to retrieve the optical phase information of the sample. This task has been usually performed by stages with great success, but presents the inconvenient of requiring a series of sequential shots of the object under study. Time-varying phase distributions are excluded from this schema and a single-shot PSI technique needs to be used. The most common single-shot PSI technique is based on polarization principles to modulate the phase-shift of the interferograms. The aim of this thesis is to present novel interferometric configurations based on polarization phase shifting techniques.

Theoretical considerations for the polarization-interferometric properties are used to successfully analyze dynamically phase changes in time varying samples. This approach has given birth to several advanced interferometric systems applied to common path configurations, slope phase measurements, temperature profiles and also proposes new configurations. Experimental results for dynamic and static transparent samples are presented.

Acknowledgements

I would like to express my deep gratitude to Prof. Amalia Martínez for giving me the opportunity to do the PhD under her esteemed guidance. My sincere thanks are due to her for providing me freedom and opportunities to expand my research horizons.

I also would like to express my deep gratitude to Prof. Noel Iván Toto Arellano; his encouragement played a crucial role in accomplishing the objectives that we had set for this thesis. I am also grateful to his family members Mrs. Patricia and Damian for their moral support.

I would like to thank the Mexican Science Council (CONACYT) for supporting me with a PhD. scholarship for the period 2011-2014. This research was supported by CONACYT under grant 180449.

I take this opportunity to thank Prof. Yukitoshi Otani for the support and guidance provided during my stay at The Center for Optical & Research and Education in Utsunomiya University in Japan.

I am grateful to my parents, brothers, and my wife Geliztle for everything that I may have attained in my life.

Contents

Introduction

Optical measurement techniques have become indispensable tools in many areas of science and engineering. The whole-field, non-contact and highly accurate measurement capabilities are among the principal features of these techniques. These techniques encode the information on the measure in the phase of a two-dimensional fringe pattern; several phase shifted replicas of this fringe pattern are used for retrieve information of the sample.

Phase shifting techniques are often used in optical interferometry[1], fringe projection profilometry[2,3], digital holography[1,4], electronic speckle pattern interferometry and shearography[5,6] because they allow to analyze samples using non-contact techniques with high accuracy. The use of phase shifting modulated by polarization has the advantage of not requiring mechanical components, such as a piezoelectric transducer (PZT), to obtain the phase shifts, since it decreases the sensitivity of the system against external vibrations. A common optical system uses linear polarizing filters and birefringent quarter-wave plates to achieve modulation[7,8].

The main purpose of Dynamic Phase-Shifting Interferometry (DPSI) is to collect all the phase-shifted data in a single exposure in order to minimize time-varying environmental effects. Since the data are collected simultaneously, the effects of vibration and turbulence are greatly reduced.

Some DPSI systems achieve the simultaneous capture of several interferograms by means of polarization, such as through the use of micro-polarizer array elements[9], a point diffraction interferometer[10], a two-window phase grating interferometer[11], as well as through the use of a liquid-crystal spatial modulator[12], among others. These systems have been employed in several fields of application[13,14].

Single shot polarization phase shifting techniques are currently a focus field of study, the most important and an industry standard nowadays are the pixelated phase mask (PPM) interferometers. One of the properties of these systems is that the modulating phase-mask

remains fixed, this placed before the CCD light sensor[15]. Some authors nowadays presents novel algorithms based on these limitations, for example in the demodulation form, algorithms focused on harmonic rejections and recently encountered a more accuracy results by proposing an extension of the phase-shifting unit cell[16,17].

The heart of the PPM interferometry systems lies in a pixelated phase-mask where each pixel has a unique phase-shift. A small number of discrete steps (usually 4) can be arranged into a "unit cell" which is then repeated contiguously over the entire array. The unit cell can be thought as a super-pixel; the phase across the unit cell is assumed to have the same value. Figure 0.1 illustrates a unit cell comprised of four discrete phase steps. The overall system consists of a polarization interferometer that generates a reference wavefront **R** and a test wavefront **T** having orthogonal polarization states (which can be linear or circular) with respect to each other. The pixelated phase-mask (PPM) and the detector array may be located in the same image plane, or positioned in conjugated image planes of the PPM and the detector array. For example, the PPM located at the output of the polarization interferometer and then an imaging system in charge to re-image the light transmitted through the PPM onto the detector array.[18]

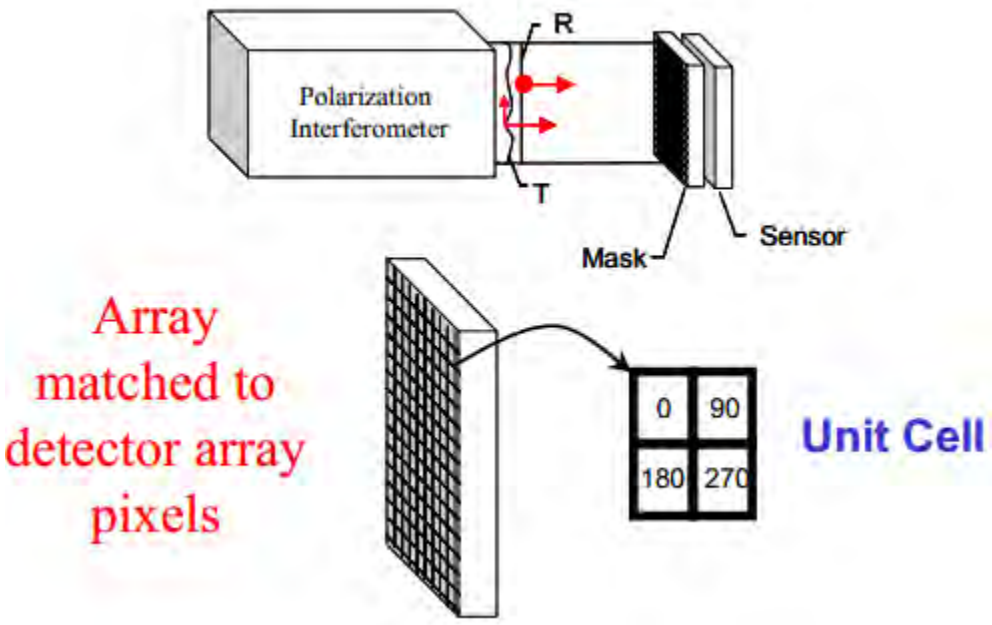

Figure 0.1 Basic concept of the pixelated phase mask interferometer.

Alternative systems, based on phase shifting polarization techniques, have been presented before[19]. These systems can obtain interference replicas by using phase/amplitude gratings[20,21] but can retrieve only the phase data map.

In this research, several single shot phase shifting interferometers are proposed taking into account the interferometric and polarization phase shifting properties in order to present some alternatives to the PPM interferometer.

Thesis Objectives

1. Present the theoretical background used for single shot phase shifting interferometers starting from the polarization properties through the Jones Calculation approach and ending with the interferometric replication involved using a 4-f system with a phase/amplitude grating in its Fourier plane.
2. Propose several interferometric systems in order to follow the 4D profiles of phase objects. Configurations based on retrieving the slope of the phase directly; dynamic temperature field measurements and configurations avoiding the use of the 4-f system with phase/amplitude gratings are proposed.

Outline of the Thesis

Chapter 1 introduces the concepts of single shot phase shifting interferometry techniques based on polarization modulation and interference replication using a 4-f system with phase/amplitude grating.

Chapter 2 introduces a quasi-common path interferometer based on the interference between replicas of the reference and object beams. The system geometry itself takes into account the separation of the input beams and also the corrections involved in the usage of polarization components that works at different wavelength than the light source used.

Chapter 3 presents a system capable of retrieving the slope phase object directly.

Chapter 4 is focused on analyzing the temporal temperature variation of a thin-flame implementing new calibration and fringe processing techniques.

Chapter 5 is to propose a configuration that avoids the usage of a 4-f system with a grating in the Fourier plane as a replication system. The system considers the two-interferograms output of a polarization Mach-Zehnder interferometer.

Chapter 6 shows an implementation related to birefringence mapping using a pixelated phase mask camera.

The final part of the thesis presents the summary, conclusions and future work.

Chapter 1

Single Shot Phase Shifting Interferometry

Single shot phase shifting interferometer that uses polarization phase shifting techniques have three main characteristics in common:

1) The interferometer needs the reference and the object beams to have orthogonally linearly polarization states between them.[22]
2) The polarization phase shifting is controlled by the angle of polarization components (by using a linear polarizer or a half-wave plate, HWP)[23–26].
3) The interferograms replication system which assesses the phase shifted interferograms in the image plane.[10,19,8]

The first consideration can be achieved by taking into account the polarization properties of the implemented interferometer. For simplicity the Jones calculus approach will be used to follow the polarizing state in each stage of the interferometer. Figure 1.1 presents a Polarizing Mach-Zehnder (PMZ) interferometer fulfilling this condition.

At the entrance of the interferometer a half-wave retarder and a linear polarizer at 45°, LP_{45°, are used to have a 45° linearly polarized input beam, $\vec{J}_{in} = \frac{1}{\sqrt{2}}\begin{pmatrix}1\\1\end{pmatrix}$. Taking the polarizing beam splitter (PBS) as a linear polarizer at 0° and 90° for the transmitted and reflected part, the output state of the PMZ:

$$\vec{J}_{out} = \vec{J}_{ref} + \vec{J}_{obj},$$
$$\vec{J}_{out} = \frac{1}{\sqrt{2}}\begin{pmatrix}0\\1\end{pmatrix} + \frac{1}{\sqrt{2}}\begin{pmatrix}e^{i\varphi(x,y)}\\0\end{pmatrix} \quad 1.1$$

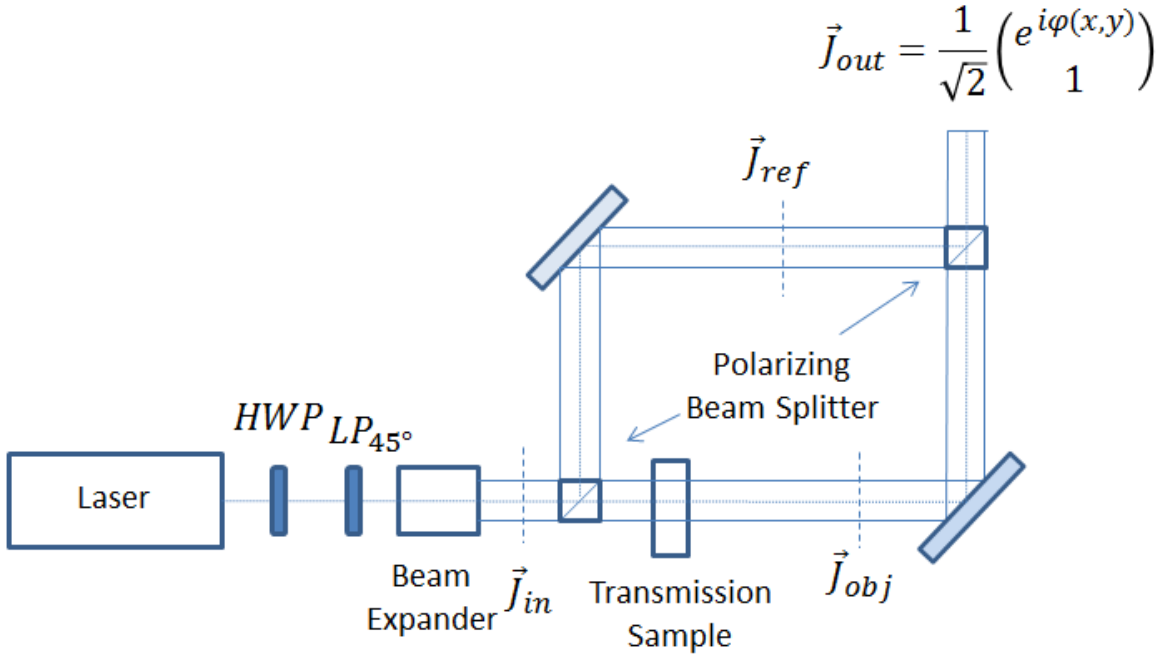

Figure 1.1 Polarizing Mach-Zehnder (PMZ) interferometer.

where $\vec{J}_{ref}$ and $\vec{J}_{obj}$ represents the state corresponding to the reference and object beams:

$$\vec{J}_{obj} = \begin{bmatrix} 1 & 0 \\ 0 & 0 \end{bmatrix}\begin{bmatrix} e^{i\varphi_{obj}(x,y)} & 0 \\ 0 & e^{i\varphi_{obj}(x,y)} \end{bmatrix}\begin{bmatrix} 1 & 0 \\ 0 & 0 \end{bmatrix}\vec{J}_{in}$$
$$\vec{J}_{ref} = \begin{bmatrix} 0 & 0 \\ 0 & 1 \end{bmatrix}\begin{bmatrix} e^{i\varphi_{ref}(x,y)} & 0 \\ 0 & e^{i\varphi_{ref}(x,y)} \end{bmatrix}\begin{bmatrix} 0 & 0 \\ 0 & 1 \end{bmatrix}\vec{J}_{in}. \quad 1.2$$

By assuming $\varphi_{ref} = 0$, $\varphi_{obj} = \varphi$. It is important to note that the transparent sample is treated only as a phase object. For a more rigorous treatment, the Jones matrix of the sample need to be taken into account and polarization compensation components need to be placed on the reference beam.

For a correct implementation of the system and to avoid the use of more specialized polarization components, double reflection and transmission of the beams is carried out. To do this, Figure 1.2 presents two common interferometry configurations: a cyclic path shearing interferometer and a Michelson interferometer fulfilling this condition to apply the polarization phase shifting conditions.

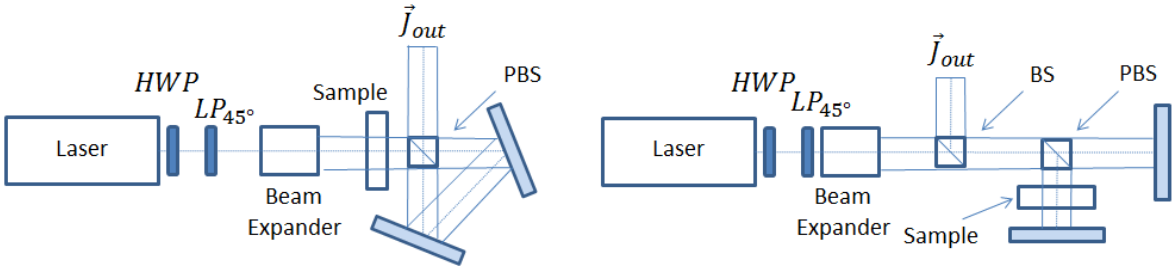

Figure 1.2 Cyclic path shearing interferometer and a Michelson interferometer employing polarization.

1.1 Polarization Phase Shifting Techniques

It is often useful to be able to shift the location of the fringes when displaying an interferogram. In conventional interferometry, we move the fringes by changing the relative phase between the interfering waves[23]. The most common system is the use of a piezoelectric transducer (PZT) which translates a mirror perpendicularly to its surface. There also exists another class of fringe shifter employing polarization techniques. The most common techniques are based on controlling the phase shift by rotating polarization components such as linear polarizers or half-wave retarders placed at the output of the interferometer whose reference and object beams have orthogonal linear polarization states.

Figure 1.3 shows a diagram of the phase shifter that could be used at the exit of an interferometer where the reference and test beams have orthogonal linear polarization. A quarter-wave plate converts one of the two interfering beams into right-handed circularly polarized beam and the second interfering beam into a left-handed circularly polarized beam. As a polarizer is rotated an angle θ the phase difference between the test and reference beams changes by 2θ. The polarizer also makes it possible for the two beams to interfere. The output polarization state of a beam, after passing through a linear polarizer at angle θ, can be obtained as:

$$\vec{J}_{\theta} = LP_{\theta} \cdot QWP_{45°} \cdot \vec{J}_{in}$$

$$\vec{J}_{\theta} = \begin{bmatrix} cos^2\theta & cos\theta sin\theta \\ cos\theta sin\theta & sin^2\theta \end{bmatrix} \cdot \frac{1}{\sqrt{2}} \begin{bmatrix} 1 & i \\ i & 1 \end{bmatrix} \cdot \begin{bmatrix} e^{i\varphi(x,y)} \\ 1 \end{bmatrix}. \quad 1.3$$

Its corresponding intensity will results in the well-known interferogram equation with a controlled phase shift twice the angle of the polarizer,

$$I_\theta = \left\|\vec{J}_\theta\right\| = 1 + \sin[(\varphi(x,y) + 2\theta)], \qquad 1.4$$

Figure 1.4 presents a polarization Mach-Zehnder (PMZ) interferometer as an example.

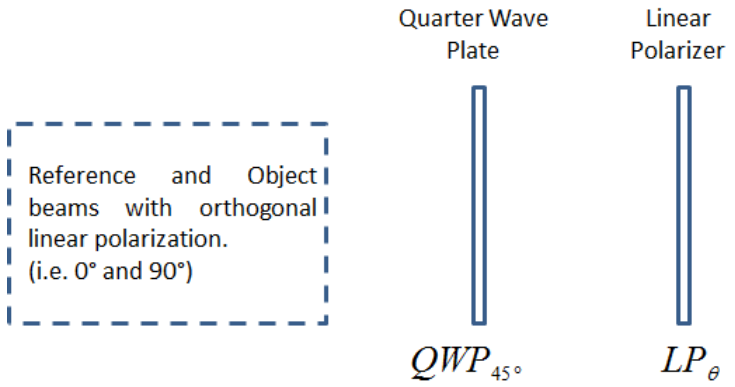

Figure 1.3 Polarization phase shifter controlled by the angle of the linear polarizer.

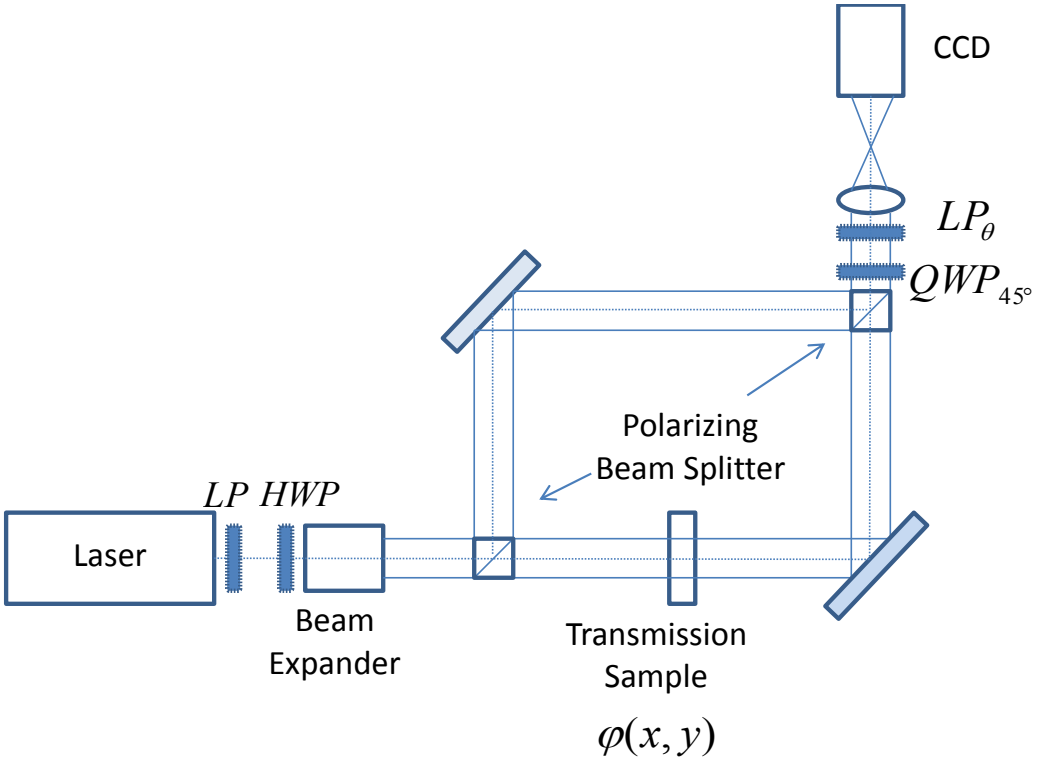

Figure 1.4 Mach-Zehnder interferometer where the phase shift is controlled by the angle of the linear polarizer, LP_θ, placed at the exit of the interferometer

An alternative polarization phase shift system is implemented by changing the angle of a half-wave plate placed between two quarter wave plates and a fixed polarizer at the exit of the interferometer. In this case the phase shift introduced will be fourth times the angle of the half-wave plate [22,24]

1.2 Interference Pattern Replication

When the interferometer is coupled to a 4-f system using phase grids or Bi-Ronchi gratings, it is possible to obtain replicas of the interference pattern. Each of these replicas can be modulated by polarization. Figure 1.5 represents a schematic diagram of the 4-f system with a grating $G(\mu,\nu)$ placed in the frequency plane in order to get replicas of the input polarization state $\vec{J}_{Tot} = \vec{J}_{obj} + \vec{J}_{ref}$. In this case the linear polarizer LP is placed on each of the replicas obtained.

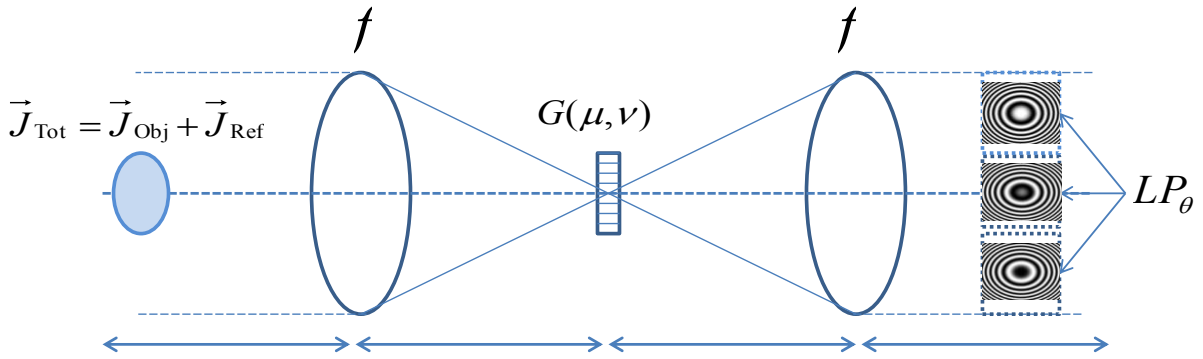

Figure 1.5 Replication system composed by a 4-f system with a grating $G(\mu,\nu)$ placed in the frequency plane in order to get replicas of the input polarization state.

The output interferogram, I_{out}, will corresponds to the convolution of the diffraction pattern of the grating, $G(\mu,\upsilon)$, with the interefrogram, $I_\theta(x,y)$,

$$I_{out} = I_\theta(x,y) * \left|\widetilde{G(\mu,\upsilon)}\right|; \qquad 1.5$$

depending of the characteristics of the grating, certain properties will be encountered in the replicated interferogram. In this work we used amplitude (Ronchi Ruling) and phase gratings commercially available[27,28].

For explanation purposes, the case with a sinusoidal amplitude grating will be discussed. Its complex amplitude is:

$$\begin{aligned} G(\mu,\nu) &= \frac{1}{2}[1 + m\cos(2\pi X_0\mu + \varphi_i)] \\ &= \tfrac{1}{2} + \tfrac{m}{4}e^{i(2\pi X_0\mu+\varphi_i)} + \tfrac{m}{4}e^{-i(2\pi X_0\mu+\varphi_i)}, \end{aligned} \tag{1.6}$$

with m being the grating contrast and $X_0 = \lambda f/d$ with d as the grating period. Its corresponding Fourier transform is given by

$$\widetilde{G(\mu,\upsilon)} = \tfrac{1}{2}\delta(x,y) + \tfrac{m}{4}e^{i\varphi_i}\delta(x - X_0, y) + \tfrac{m}{4}e^{-i\varphi_i}\delta(x + X_0, y), \tag{1.7}$$

with $\delta(x,y)$ as the two-dimensional Dirac delta function. By taking eq. 1.5:

$$\begin{aligned} I_{out} &= I_\theta(x,y) * \left|\tfrac{1}{2}\delta(x,y) + \tfrac{m}{4}e^{i\varphi_i}\delta(x - X_0, y) + \tfrac{m}{4}e^{-i\varphi_i}\delta(x + X_0, y)\right| \\ &= \tfrac{1}{2}I_\theta(x,y) + \tfrac{m}{4}I_\theta(x - X_0, y) + \tfrac{m}{4}I_\theta(x + X_0, y). \end{aligned} \tag{1.8}$$

Thus, at the image plane of the 4-f system three replicas of the interferogram will be encountered.

Pattern Replication using Amplitude Gratings

In general, when Bi-Ronchi gratings are placed in the Fourier plane, they can be considered to be the multiplication of two cross amplitude Ronchi gratings[19],

$$G(\mu,\nu) = G(\mu)\cdot G(\nu) = \sum_{n=-N}^{N} rect\left[\frac{\mu - n\cdot d_\mu}{a_{w\mu}}\right]\cdot\sum_{l=-L}^{L} rect\left[\frac{\nu - l\cdot d_\upsilon}{a_{w\mu}}\right], \tag{1.9}$$

where N, L are the numbers of components of the grating, d_μ, d_υ are the respective periods along directions "μ" and "ν", and $a_{w\mu}$, $a_{w\nu}$ are the widths of the light part of the strips along each direction. The gratings studied have equal periods in both directions; then, $d_\mu = d_\upsilon = d$, so $a_{w\mu} = a_{w\upsilon} = a_w$. Due to the convolution properties of the Fourier transform[30], the corresponding spectrum is:

$$\begin{aligned}\tilde{G}(x,y) &= \tilde{G}(x)\cdot\tilde{G}(y)\\ &= \frac{a_w^{\,2}}{d^2}\sum_{n=-N}^{N}\operatorname{sinc}\left(\frac{a_w}{d}\cdot x\right)\delta\left(x-\frac{n}{d}\right)\sum_{l=-L}^{L}\operatorname{sinc}\left(\frac{a_w}{d}y\right)\delta\left(y-\frac{l}{d}\right),\\ &= \sum_{n=-N}^{N}C_{xn}\delta\left(x-\frac{n}{d}\right)\sum_{l=-L}^{L}C_{yl}\delta\left(y-\frac{l}{d}\right)\end{aligned} \tag{1.10}$$

with $C_{xn}=\frac{a_w}{d}\operatorname{sinc}\left(\frac{a_w}{d}\cdot x\right)$ and $C_{yl}=\frac{a_w}{d}\operatorname{sinc}\left(\frac{a_w}{d}\cdot y\right)$.

For the experimental case where gratings have the same period, $d=0.01\ mm$, the diffraction patterns generated, using Eq. 1.10, are shown in Figure 1.6. Figure 1.6(a) shows the simulated diffraction pattern generated by the Bi-Ronchi grating. In Figure 1.6(b), it can be seen that the amplitude spectra for each axis shows more than three orders of diffraction; however, only orders 0 and ±1 allow one to obtain replicas of the interference pattern with comparable intensities.

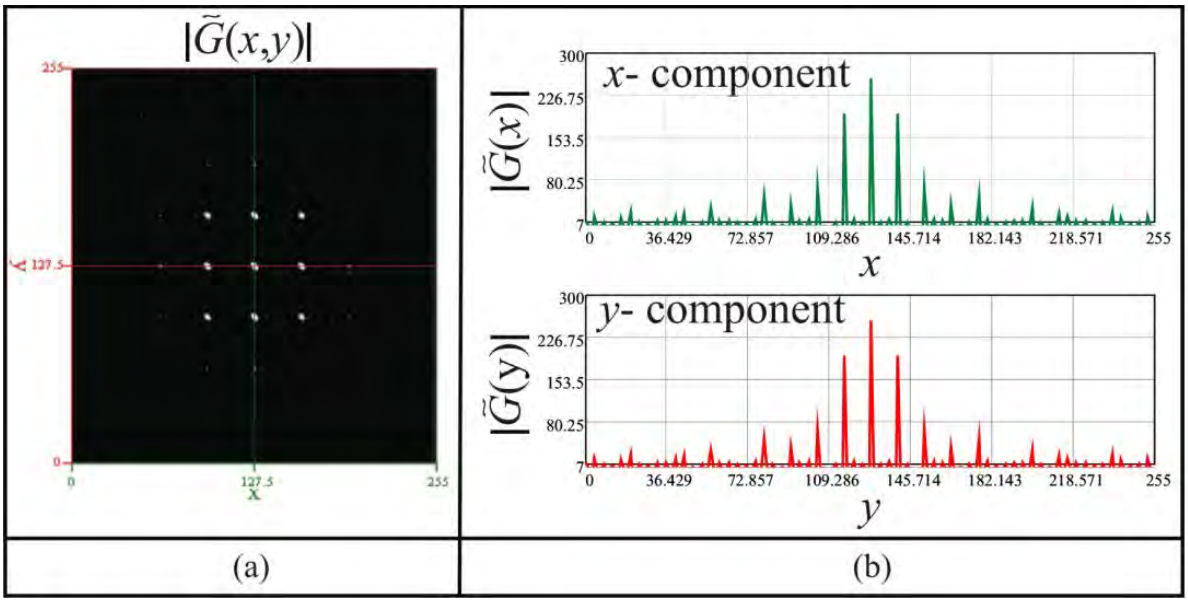

Figure 1.6 Simulated diffraction pattern generated by high frequency Bi-Ronchi gratings. (a) Diffraction spectra. (B) x-y components of diffraction spectra of each grating component.

The 4-*f* system with high frequency Bi-Ronchi gratings only multiplexes the interference pattern generated at the output of interferometer; the phase shifts in the

interference pattern are managed only by linear polarizers placed at the output. Considering Eq. 1.4 the interference pattern $I'(x,y)$ on the image plane of the system is

$$\begin{aligned} I'(x,y) &= \left| LP_{\psi}\left[\vec{J}_{Obj} + \vec{J}_{ref}\right] * \widetilde{G}(x,y)\right|^2 \\ &= I_{out}(x,y) * \left|\widetilde{G}(x,y)\right|^2 \end{aligned} . \qquad 1.11$$

As in Eq. 1.3, each beam has circular polarization, LP_{ψ} represents the Jones matrix of the linear polarizer at angle ψ and $I_{out}(x,y)$ represents the interference pattern generated by the interferometer. The resulting intensity captured by the camera is:

$$\begin{aligned} I'(x,y) &= \sum_{n=-N}^{N}\sum_{l=-L}^{L} {C_{yl}}^2 {C_{xn}}^2 I\left(x - \frac{n}{d_x}, y - \frac{l}{d_y}\right) \\ &= \sum_{n=-N}^{N}\sum_{l=-L}^{L} {C_{yl}}^2 {C_{xn}}^2 \left\{1 + \cos\left[\varphi(x,y) + 2\cdot\psi\right]\right\} \end{aligned} . \qquad 1.12$$

Equation 1.12 shows that the resulting intensity distribution consists of replicas of the pattern generated by the interferometer displaced to the n^{th} and l^{th} orders of diffraction; each replica of the main pattern maintains an intensity modulated by the Fourier coefficients C_n and C_l corresponding to each direction. In this case the Ronchi gratings only multiplex the pattern, so the amplitudes of the orders only increase or decrease the intensity of the interference patterns, as it's shown in Figure 1.7. Figure 1.7 shows the experimental results obtained with a Bi-Ronchi grating. The interference patterns used, enclosed in a circle, with independent phase shifts, can be generated by linear polarizers. Figure 1.7(a) shows the diffraction orders distribution, indicated by two subscripts. Figure 1.7(b) shows the diffraction orders generated by the grating; it can be seen that they have at least 4 diffraction orders with comparable intensities. This result is due to the modulation generated by coefficients C_n and C_l (see Eq. 1.12). Figure 1.7(c) shows the replicas of the interference patterns centered on each diffraction order.

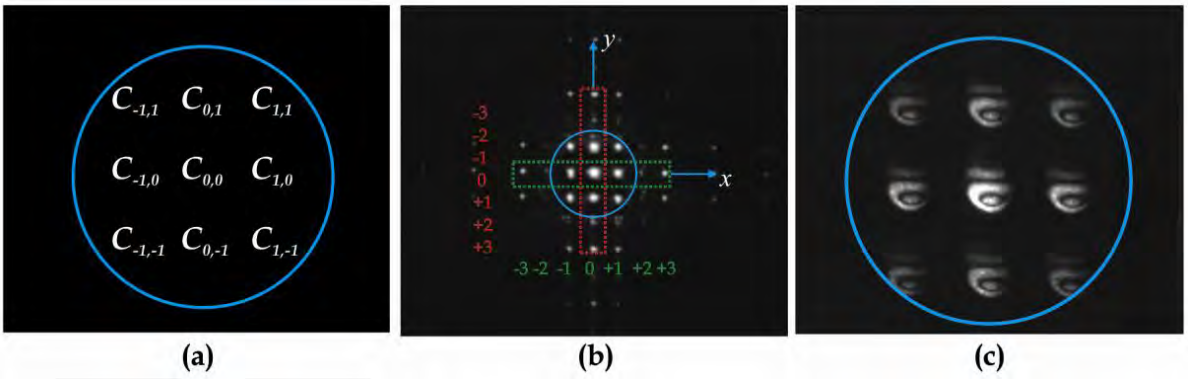

Figure 1.7 Replicas of the interference patterns. (a) Fourier coefficients for each replica of the interference pattern. (b) Experimental diffraction orders generated by high frequency Bi-Ronchi gratings (100 *ln/mm*). (c) Replicas of the interference patterns centered on each diffraction order (Circle).

Pattern Replication using Phase Gratings

A sinusoidal phase grid generated by multiplication of two sinusoidal phase gratings, whose respective grating vectors are crossed, generates diffraction orders modulated by Bessel functions J_q and J_r [21], and the image of the interference pattern generated by the interferometer is found centered around each of them.

To draw theoretical conclusions, we assume that the phase grid is made up from two phase gratings of modulation depth as $2\pi A_g$ each and with orthogonal gratings vectors. Taking the rulings of one grating along the "μ" direction and the rulings of the second grating along the "ν" direction, the resulting Fourier transform of the centered phase grid can be written as:

$$\tilde{G}_2(x,y)=\sum_{q=-\infty}^{q=\infty}\sum_{r=-\infty}^{r=\infty}J_q(2\pi A_g)J_r(2\pi A_g)\,\delta(x-qX_0,y-rX_0), \qquad 1.13$$

where the order separation is $X_0=\lambda f/d$ and J_q, J_r denotes the Bessel function of the first kind and integer order *q, r*. In the image plane of the system, taking only the contribution of an isolated term of order *qr,* the irradiance would be proportional to

$$I'(x,y)=\sum_{q=-\infty}^{\infty}\sum_{r=-\infty}^{\infty}2J_q^2J_r^2\left\{1+\cos\left[\varphi(x_q,y_r)+2\theta\right]\right\}. \qquad 1.14$$

where a translation of coordinates was used around the order position ($x_q = x - qX_0$ and $y_r = y - rX_0$). As before the obtained phase shift is twice the angle of the linear polarizer.[31] The grid makes copies of both interfering beams, keeping their circular polarizations to be detected through a linear polarizer array, where each of the linear polarizer is set at different angle.

Figure 1.(a) shows the diffraction orders distribution, indicated by a subscript $J_{n,l}$, generated by the phase grid. Figure 1.8(b) shows the diffraction orders obtained and it can be seen that they have at least 9 diffraction orders with comparable intensities. This result is due to the modulation generated by Bessel function $J_{n,l}$. Figure 1.8(c) shows the replicas of the interference patterns obtained centered on each diffraction order.

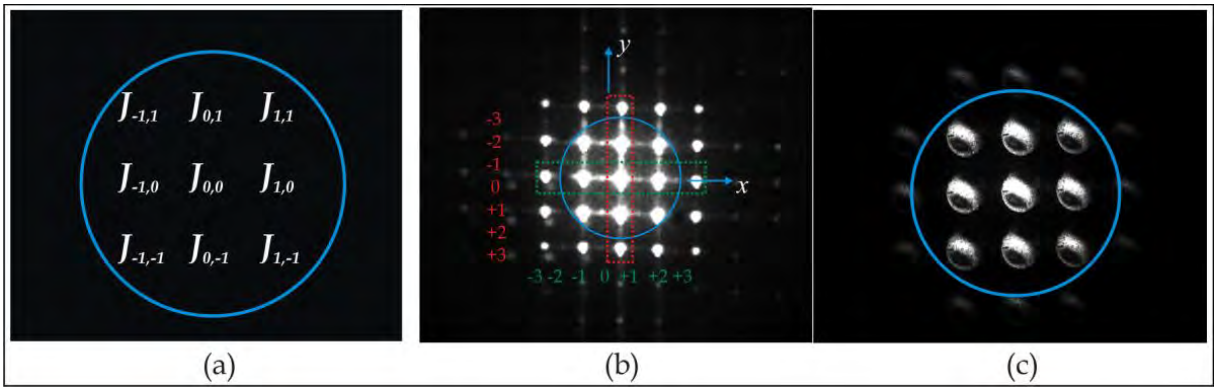

Figure 1.8 Replicas of the interference patterns. (a) Fourier coefficients for each replica of the interference pattern. (b) Experimental diffraction orders generated by high frequency phase gratings (110 *groves/mm*). (c) Replicas of the interference patterns centered on each diffraction order (Circle).

1.3 Conclusion

Polarization phase shifting techniques requires several conditions that need to be met, the most important is that the interferometer needs to have linear orthogonal polarization states between the reference and object beams.

By using the 4-f system with gratings placed in the frequency plane, as a replication system, an amplitude modulation is obtained in the image plane; this latter effect can be compensated by using normalization procedures or by using replicas orders with almost the same amplitudes.

Chapter 2

4D Phase Profiles based on a quasi-common path configuration

In this chapter, we propose a configuration of a two-window polarizing phase shifting interferometer[11,20,32], based on two coupled systems: a Mach-Zehnder interferometer(MZI) that allows the two-window generation with adjustable separation, and a 4-*f* system with phase gratings placed on the frequency plane.[19,33] One advantage of these configurations is that, when the beam separation is properly changed, interference of the different diffractions orders can be obtained. The system is insensitive to external vibrations due to its quasi-common path configuration. The previously presented two-window interferometer with diffraction gratings[33] was implemented using a fixed separation corresponding to the grid used. In the proposed configuration, we can freely adjust these separation and positions. Also, with the proposed optical system, we can obtain results of the same quality as those obtained in previous reports[20,33], in a more flexible system which is not limited by optical components, such as the grid used.

To generate independent phase shifts in the interference patterns, a linear polarizer is placed at a convenient angle on each replica[8]. In the experimental results presented, the interference patterns are processed by means of two methods, for the case of four interferograms and for the case of nine interferograms, using the symmetrical (*N*+1) nine algorithm[34].

2.1 Phase Grating Interferometry

Phase gratings have interesting properties, such as the advantage of using a higher percentage of incident energy compared with absorption gratings. The advantage of using cross-phase gratings is the ability to generate up to 16 replicas of the interferogram with independent phase shifts. This allows the use of other algorithms to process the phase. Furthermore, the use of cross-phase gratings allows obtaining π-phase shifts, figuring 2.1, simplifying the polarizer arrangement. A phase grid, carefully constructed by means of superposing two phase gratings with their respective grating vectors at $\pm 90°$, is placed at the system's Fourier planes. Taking the rulings of one grating along the direction, $\mu = \frac{u}{\lambda f}$, and the rulings of the second grating along the $\upsilon = \frac{v}{\lambda f}$ direction, the resulting centered phase grid can be written as:

$$G(\mu,\upsilon) = e^{i2\pi A_g \sin[2\pi \cdot X_0 \mu]}\, e^{i2\pi A_g \sin[2\pi \cdot X_0 \upsilon]}$$
$$= \sum_{q=-\infty}^{\infty} J_q(2\pi A_g) e^{i2\pi \cdot qX_0 \mu} \sum_{r=-\infty}^{\infty} J_r(2\pi A_g) e^{i2\pi \cdot rX_0 \upsilon}, \qquad 2.1$$

where the frequencies along each axis direction are taken as X_0, with $2\pi A_g$ being the phase grating amplitude, and J_q and J_r the Bessel functions of the first kind of integer order *q, r*, respectively. The Fourier transform of the phase grid becomes

$$\tilde{G}(x,y) = \sum_{q=-\infty}^{q=\infty} \sum_{r=-\infty}^{r=\infty} J_q(2\pi A_g) J_r(2\pi A_g)\, \delta(x - qX_0, y - rX_0), \qquad 2.2$$

which consists of point-like diffraction orders distributed on the image plane. Phase grid interferometry is based on a two crossed phase grating placed as the pupil in a 4-*f* Fourier optical system, figure 2.2. A convenient window pair for a grating interferometer implies an amplitude transmittance given by

$$O(x,y) = A(x + \frac{x_0}{2}, y) + B(x - \frac{x_0}{2}, y), \qquad 2.3$$

where x_0 is the separation from center to center between two beams, $A(x, y)$ as the reference beam aperture and $B(x,y)$ is the beam aperture where the phase object is placed. Placing a

grating of spatial period $d = \lambda f / X_0$ at the Fourier plane, with a corresponding transmittance given by $G(\mu,\upsilon)$, Eq. 2.1. The image formed by the system consists basically of replications of each window separated at distances X_0. This image is defined by $O'(x,y)$; that is, the convolution of $O(x,y)$ with the Fourier transform of the phase grating, $\tilde{G}(x,y)$ represented by

$$\begin{aligned} O'(x,y) &= O(x,y) * \tilde{G}(x,y) \\ &= w\left(x + \frac{x_0}{2}, y\right) * \sum_{q=-\infty}^{\infty} J_q(2\pi A_g)\,\delta(x - qX_0, y) \\ &+ \left[w\left(x - \frac{x_0}{2}, y\right) e^{i\phi\left(x-\frac{x_0}{2},y\right)} \right] * \sum_{q=-\infty}^{\infty} J_q(2\pi A_g)\,\delta(x - qX_0, y). \end{aligned} \quad , \qquad 2.4$$

where (*) denotes the convolution. By adding the terms of Eq. 2.4, taking *q* and *q-1* (both located within the same replicated window $w\left(x - qX_0 + \frac{x_0}{2}, y\right)$), and for the case of matching the beams positions with the diffraction order's positions ($X_0 = x_0$), Eq. 2.4 can be simplified as

$$O'(x,y) = \sum_{q=-\infty}^{\infty} \left[J_q(2\pi A_g) + J_{q-1}(2\pi A_g) e^{i\phi\left(x - x_0\left[q-\frac{1}{2}\right], y\right)} \right] w\left(x - x_0\left[q - \frac{1}{2}\right], y\right). \qquad 2.5$$

Thus, an interference pattern between fields associated to each window must appear within each replicated window. The fringe modulation m_q of each pattern would be of the form[32]

$$m_q = \frac{2J_q J_{q-1}}{J_q^2 + J_{q-1}^2}, \qquad 2.6$$

where each fringe contrast depends on the relative phases between the Bessel functions J_q.

2.2 Phase shifting interferometry with modulation of polarization

Turning the attention to gratings, in order to introduce additional phase shifts in the interference pattern centered around $(x_0[(q-(1/2)],y)$, each of the windows is illuminated with different polarizations using retarding plates Q_R and Q_L, Figure 2.2; this arrangement introduces Jones polarization vectors $\vec{J}_R$ and $\vec{J}_L$ into the interference terms of Eq. 2.4. After placing a linear polarizing filter with the transmission axis at an angle ψ, its irradiance turns out to be proportional to:

$$\left\|\vec{J}_T\right\|^2 = A(\xi,\alpha')\left\{\left(J_q{}^2 + J_{q-1}{}^2\right) + 2J_qJ_{q-1}\cos[\xi(\psi,\alpha') - \phi(x,y)]\right\}, \qquad 2.7$$

where $\vec{J}_T = J_\psi^l \vec{J}_L J_q + J_\psi^l \vec{J}_R J_{q-1}$, J_ψ^l is the transmission matrix for the linear polarizer at angle ψ, $\pm\alpha'$ is the retardation of each plate, and $\xi(\psi,\alpha')$ denotes the phase shifting term induced by modulation of polarization given by

$$\xi(\psi,\alpha') = ArcTan\left[\frac{\sin[2\psi]\cdot\sin[\alpha'] + \sin^2[\psi]\cdot\sin[2\alpha']}{\cos^2[\psi] + \sin^2[\psi]\cdot\cos[2\alpha'] + \sin[2\psi]\cdot\cos[\alpha']}\right], \qquad 2.8$$

$A(\psi,\alpha')$ is defined as

$$A(\psi,\alpha') = 1 + \sin[2\psi]\cos[\alpha'] \qquad 2.9$$

denoting each pattern as

$$\left\|\vec{J}_i\right\|^2 = A(\xi,\alpha')\left\{\left(J_q{}^2 + J_{q-1}{}^2\right) + 2J_qJ_{q-1}\cos[\xi(\psi_i,\alpha') - \phi(x,y)]\right\} \qquad 2.10$$

with $i = 1\ldots N$.

For phase-shifting interferometry with four patterns, four irradiances can be used, each one taken at a different ψ angle. The relative phase can be calculated as:[34]

$$\tan\phi = \frac{\left\|\vec{J}_1\right\|^2 - \left\|\vec{J}_3\right\|^2}{\left\|\vec{J}_2\right\|^2 - \left\|\vec{J}_4\right\|^2}, \qquad 2.11$$

where $\left\|\vec{J}_1\right\|^2$, $\left\|\vec{J}_2\right\|^2$, $\left\|\vec{J}_3\right\|^2$ and $\left\|\vec{J}_4\right\|^2$ are the intensity measurements with the values of ψ such that $\xi(\psi_1) = 0, \xi(\psi_2) = \pi/2, \xi(\psi_3) = \pi, \xi(\psi_4) = 3\pi/2$ respectively. Note that $\xi(\psi,\pi/2) = 2\psi$ and $A(\psi,\pi/2) = 1$, so a good choice for the retarders is quarter-wave retarders, as it is well

known. Dependence of ϕ on the coordinates of the centered point has been simplified to x,y. The same fringe modulation m_q results, as in Eq. 2.6. Therefore, the discussion about fringe modulation given in previous sections is retained when introducing the modulation of polarization. Such polarization modulation can be carried out also for grids, resulting in similar conclusions.

To demonstrate the use of the various interferograms obtained to extract phase under the conditions described above, we choose the symmetrical N+1 phase steps algorithms for data processing, the phase is given by[34]:

$$\tan\phi(x,y)=\frac{\sum_{i}^{N+1} I_i \sin\left(2\pi\frac{i-1}{N}\right)}{\sum_{i}^{N+1} I_i \cos\left(2\pi\frac{i-1}{N}\right)}, \qquad 2.12$$

where N+1 is the number of interferograms. For the case of nine interferograms, only five linear polarizing filters have to be placed. The transmission axes of the filter pairs LP_{i} can be the same for each one, as long as they cover two patterns with π-phase shift in between.

Experimentally, the phase shifting obtained is the result of placing a linear polarizer in each one of the interference patterns generated on each diffracting orders on the exit plane (P_i); each polarizing filter transmission axis is adjusted at a different angle ψ_i, see Figure 2.1(a). The experimental observations suggest a simplification for the polarizing filter array due to the π phase shift obtained; thus, it is not necessary to use all linear polarizing filters for all patterns. For example, in the case of four steps, we only need to place two polarizers (P_0 and P_1), each one covering two patterns with complementary phase shifts; then, $\psi_0 = 0°$ and $\psi_1 = 46.577°$ [20], which leads to phase shifts ξ of $0,\ 0,\ \pi/2,\ \pi$, and $3\pi/2$, and can be seen in Figure 2.1(b), with the dotted boxes representing the polarizing filters. This result allows us to know the phase profile. Since n-interferograms can be obtained simultaneously, the dynamic study of a phase objects can be carried out.

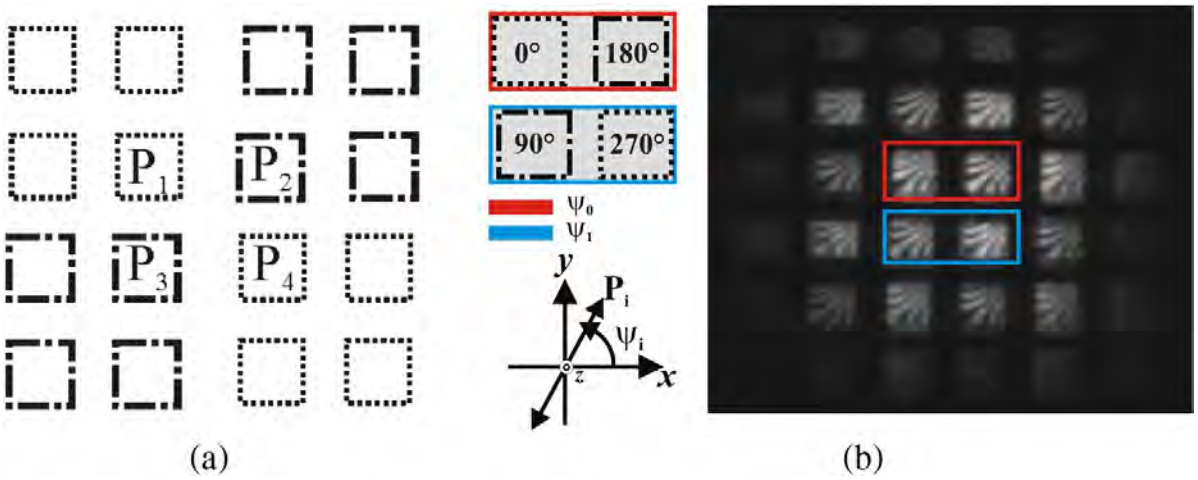

Figure 2.1 Replicas of the interference patterns obtained with the phase grid (a) Polarizing filters array. (b) Experimental interference patterns.

2.3 Experimental Setup

The optical system proposed is shown in Figure 2.2. It consists of a combination of a quarter-wave plate Q and a linear polarizing filter P_0 that generates linearly polarized light oriented at $45°$ angle entering the Mach Zehnder configuration from a YVO_3 laser operating at 532 *nm*. This configuration generates two symmetrically displaced beams by moving mirrors *M* and *M'*, enabling one to change spacing x_0 between beam centers. Two retardation plates (Q_L and Q_R), with mutually orthogonal fast axes, are placed in front of the two beams (A, B) to generate left and right nearly-circular polarized light. A phase-grating $G(u/\lambda f, v/\lambda f)$ is placed on the frequency plane (u,v) of the 4-*f* Fourier optical system that is coupled to the Mach Zehnder configuration. On plane (μ,υ), the period of *G* is denoted by *d*, and its spatial frequency by $\sigma = 1/d$. Two neighboring diffraction orders have a separation distance of $X_0 = \lambda f / d$ at the image plane for a grating; the phase shifts caused by the grating at the image plane of this system are discussed in[9,20,35].

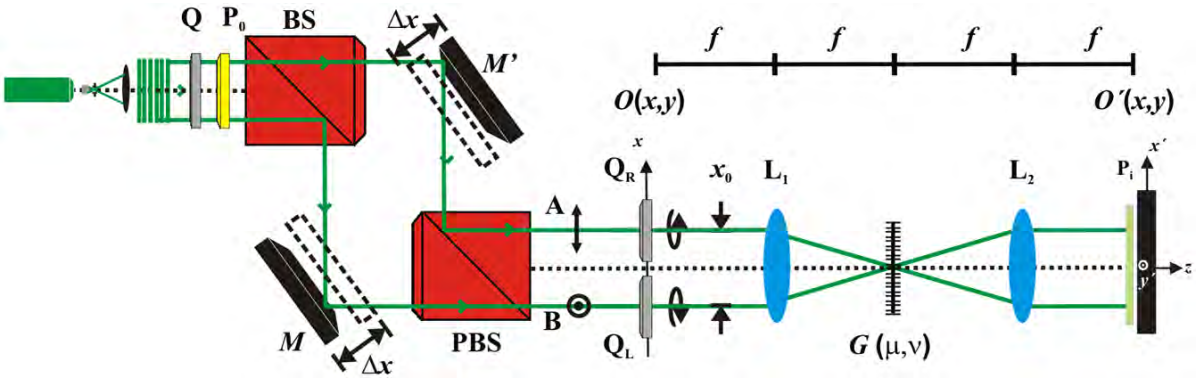

Figure 2.2 Experimental setup. BS: Beam splitter. PBS: Polarizing Beam splitter. $O(x, y)$: Object plane. $O'(x, y)$: Image plane. L_i: Lens. P_i: Polarizer's. Grating period, d = 110 *lines/mm*. x_0 = 10 *mm*. f = 150 *mm*. The transparent sample is located on *B*.

2.4 Experimental Results: Static and Dynamic Distributions

The phase gratings that were used are the commercially available ones (Edmund Optics transmission grating, dimensions: 25x25*mm*; dimensional tolerance: ± 0.5 *mm*; substrate: optical crown glass). The monochromatic camera used has a CMOS sensor with 1280 × 1024 pixels and with a pixel pitch of 6.7μm. Each interferogram was typically composed of arrays of 600 × 512 pixels and then filtered with a conventional low-pass filter to remove sharp edges and detail from the image, leaving smooth gradients and low-frequency detail. To reduce differences of irradiance and fringe modulation, each interferogram used was subjected to a rescaling and normalization process. This procedure generates patterns of equal background and equal fringe modulation. There are several 2D phase unwrapping algorithms; however for simplicity the method used for unwrapping the phase data was a non-iterative fast cosine method[36].

A phase dot generated with a magnesium fluoride film (MgF_2) on a glass substrate was placed in the path of beam B, while beam A was used as a reference; the results obtained are shown in Figure 2.3. Figure 2.3(a) shows the four patterns with $\pi/2$ phase shifts obtained in a single shot, and Figure 2.3(b) presents the phase profile of the object, in false color coding. However, more than four interferograms could be used, whether for *N*-steps phase-shifting interferometry or for averaging images with the same shift.

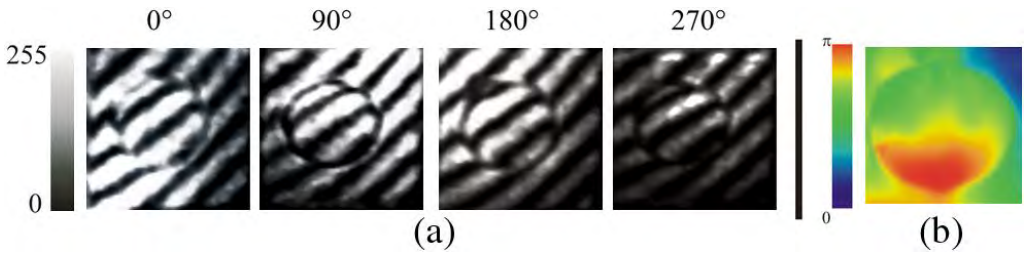

Figure 2.3 Phase dot prepared evaporating magnesium fluoride (MgF_2) on a glass substrate: (a) Four 90° phase-shifted interferograms. (b) Phase profile.

Comparatively, the results obtained with the proposed optical system, are equal to those obtained with interferometers double fixed window, however the implementation of this optical system becomes simpler, since it is easier to place the necessary components and also we are able to use phase grids with other periods, or absorption grids, only taking in consideration the correct separation of the two windows.

To demonstrate the use of several interferograms, we choose the symmetrical n=(N+1) phase steps algorithms[34], for data processing (case N=8). A constant phase shift value of $2\pi/N$ is employed when using these techniques. The phase shifts of π due to the grid spectra allow the use of a number of polarizing filters that is less than the number of interferograms, simplifying the filter array, Figure 2.4. According to Figure 2.4(b), it can be shown that for symmetrical nine, $\psi_1 = 0°$, $\psi_2 = 92.989°$, $\psi_3 = 22.975°$, $\psi_4 = 46.577°$ and $\psi_5 = 157.903°$. In this case, each resulting step corresponds to a 45° phase-shift.[32] The corresponding results and calculated phases are shown in Figure 2.5, the experimental results shows the interference pattern and unwrapped phase generated by a tilted wavefront.

A dynamic phase object is shown in Figure 2.6. It corresponds to flowing oil on a glass microscope slide allowing to flow under the effect of gravity. The phase object was put in front of **B** windows of the system of Figure 2.2. For this case, four interferograms are used to process the optical phase.

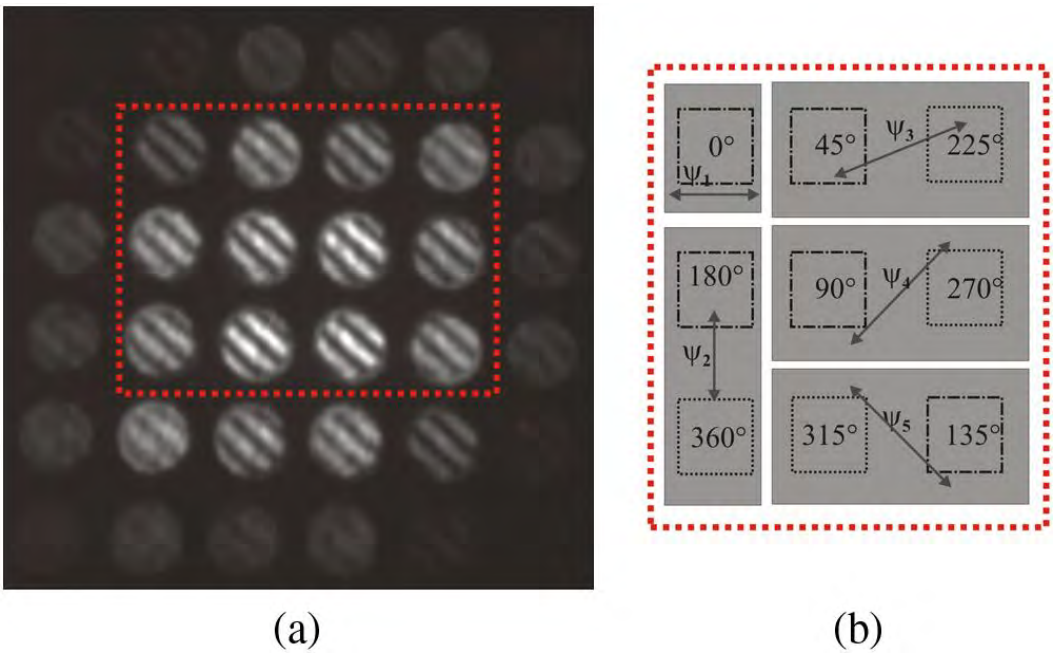

Figure 2.4 Interference patterns detected with a polarizing filter at $\psi = 25°$. (a)The interference patterns used are enclosed in the dotted rectangle. (b) Polarizer filter array for *N*=8, nine symmetrical interferograms.

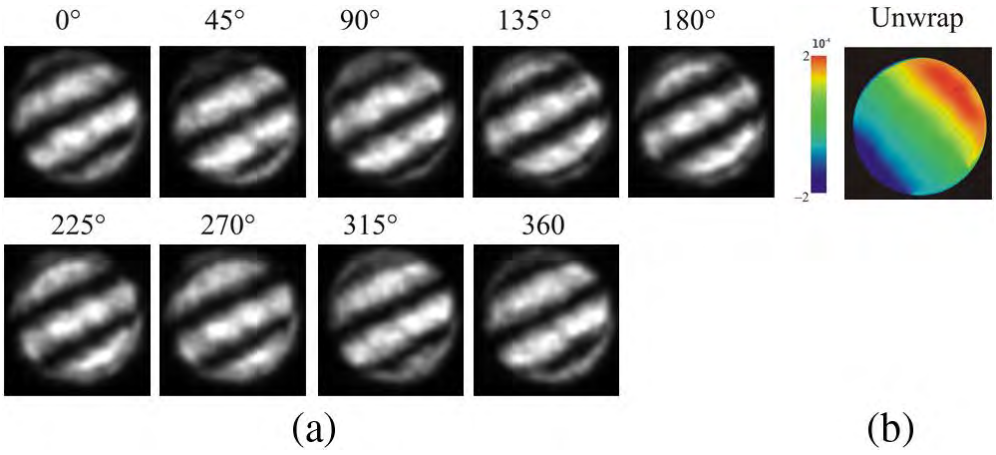

Figure 2.5 Tilted wave-front. (a) Nine 45° phase-shifted interferograms (b) Unwrapped phase data map.

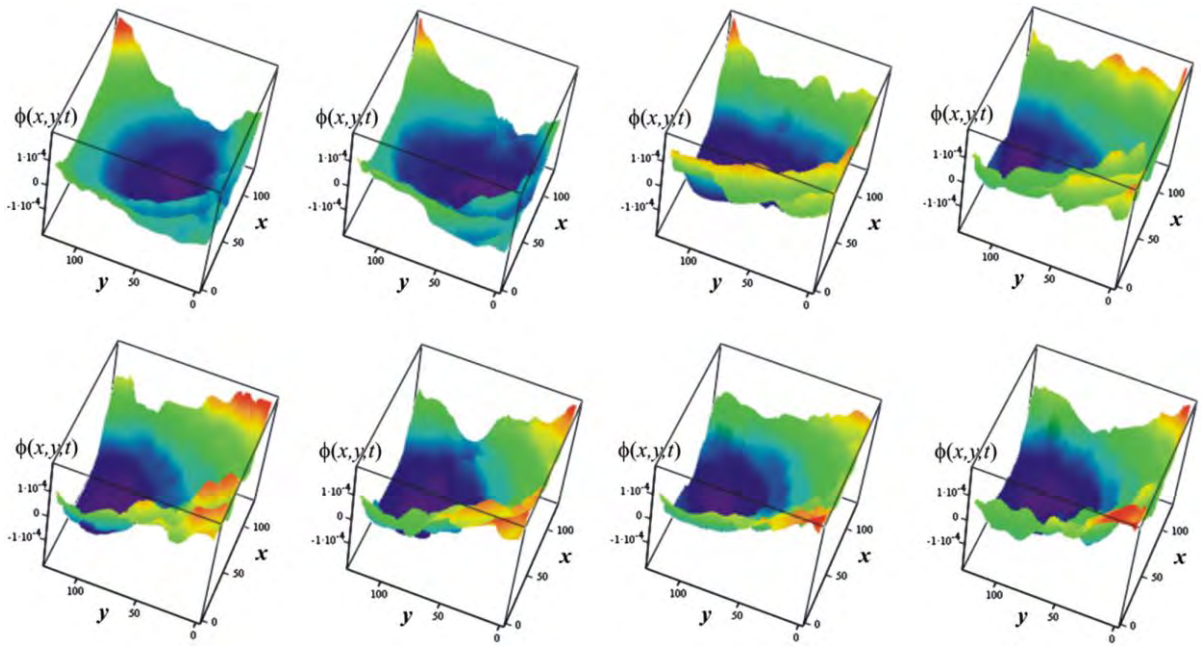

Figure 2.6 Dynamics distributions. Representative Frames. Evolution of the phase profile, one capture per 2 seconds.

2.5 Conclusion

The experimental set-up for an adjustable two windows interferometer based on a Mach Zehnder configuration has been described to obtain the phase profile of phase objects from the analysis of optical phase using polarizing phase shifting techniques. This system is able to obtain *N* interferograms with only one shot ($n \leq 16$).

Tests with four phase-shifts were presented, but also used other approaches using different phase-shifts, attained using linear polarizers with their transmission axes at the proper angle before detection (case of nine interferograms). The phase shifts of π due to the grid spectra allows the use of a number of polarizing filters which is less than the number of interferograms, simplifying the filter array. The interferometric system allows the analysis of static objects and dynamics objects.

The current system only showed the temporal evolution of an oil drop by gravity, as a future work a system capable of following specific fluid properties (viscosity, density, etc.) will be investigated.

Chapter 3

Slope Phase Measurements Interferometers

Two shearing interferometers were implemented to analyze the slope of phase objects using simultaneous phase-shifting shearing interferometry[37]. These optical configurations allow us to obtain n-shearograms simultaneously to retrieve the derivative of the optical phase data map [37,38].

In the lateral shearing interferometers the same wavefront is superposed with its copy but displaced a distance Δx. When Δx is sufficiently small, the phase difference can be approximated as the directional derivative of the wavefront in the displacement direction[39,40]. **Lateral shear interferograms** have different fields of applications like optical tests, wavefront aberrations,[41] phase singularities detection (optical vortex)[42] and mechanical stress[43] among others. In the case of **radial shear interferometers** the superposition is against the same wavefront at different scales (contracted or expanded) with no displacement. The proposed systems presents the advantage of obtaining lateral and radial shear by using of adequate components, both cases are studied and presented in this work.

Two shear interferometric systems were proposed: A cyclic path shearing interferometer and a Mach–Zehnder Radial-Shear interferometer (MZRI). Phase grid placed on a Fourier plane of a 4-f system was used as interferometric replication method.

3.1 Lateral Shear Interferometry

Defining the resultant vectorial beam amplitude of a Lateral Shear interferometer as

$$\vec{t}_1(x,y) = \vec{J}_L\, w(x-\frac{x_0}{2},y) + \vec{J}_R\, w'(x+\frac{x_0}{2},y), \qquad 3.1$$

where x_0 is the mutual separation of the beams along *x*, *w* and *w'* is the aperture of the beam sheared by a distance x_0. $\vec{J}_L$ and $\vec{J}_R$ represents the Jones vectors for right and left circular polarization as

$$\vec{J}_L = \begin{pmatrix} 1 \\ i \end{pmatrix}, \ \vec{J}_R = \begin{pmatrix} 1 \\ -i \end{pmatrix}. \tag{3.2}$$

Based on our replication method using phase gratings in a 4-f system, the two mutually separated beams enters the 4-f system with cross linear polarization, after passing a quarter-wave retarder (Q_1), cross circular polarization states are obtained. The phase grid is used to obtain replicated shearograms were each of one can be modulated by polarization to obtain the desired phase shift. The lateral shear $\Delta s = x_0$ must be smaller than the transversal section *a* of the beams, this implies that the lateral displacement is smaller than the diffraction order separation defined as X_0.

To draw theoretical conclusions, we assume that the phase grid is made up of two phase gratings (with $2\pi Ag$ the grating's phase amplitude) and with orthogonal gratings vectors. The resulting Fourier transform of the centered phase grid can be written as:

$$\tilde{G}(x,y) = \sum_{q=-\infty}^{q=\infty} \sum_{r=-\infty}^{r=\infty} J_q(2\pi A_g) J_r(2\pi A_g) \delta(x - qX_0, y - rX_0). \tag{3.3}$$

On the image plane of the system the amplitude can be written as

$$\begin{aligned} \vec{t}_0(x,y) &= \vec{t}_1(x,y) * \tilde{G}(x,y) \\ &= \sum_{q=-\infty}^{q=\infty} \sum_{r=-\infty}^{r=\infty} J_q(2\pi A_g) J_r(2\pi A_g) \left\{ \vec{J}_L \, w(x - qX_0 - \frac{x_0}{2}, y - rX_0) + \vec{J}_R \, w'(x - qX_0 + \frac{x_0}{2}, y - rX_0) \right\}. \end{aligned} \tag{3.4}$$

On the image plane of the system, a series of replicated beams can be observed. Because of their polarization, an interference pattern can be detected by placing a linear polarizer filter ($P_{\psi_{q,r}}$) at angle ($\psi_{q,r}$) before the detector on each of the (*q,r*) replicas to be used. A single fringe pattern is defined as [32]

$$I_{q,r}(x,y) = \left| P_{\psi_{q,r}} \vec{t}_0(x,y) \right|^2 = 2J_q^2 J_r^2 \left[1 + \cos\left(2\psi - \Delta\varphi(x_q, y_r) \right) \right] \tag{3.5}$$

where a translation of coordinates was used around the order position ($x_q = x - qX_0$ and $y_r = x - rX_0$), and $\Delta\varphi(x,y) = \varphi(x + x_0/2, y) - \varphi(x - x_0/2, y)$. By analyzing Eq.3.5, it can be noted that the phase shift obtained in the interferogram will be twice the angle of the linear polarizer placed and each of the interferogram amplitude modulation will be dependent of the (*q,r*) order used.

3.2 Radial Shear Interferometry

In this case the transversal sections of the beams can be described as:

$$\begin{aligned} w(x,y) &= circ\left(\frac{\rho}{M_a}\right) e^{i\varphi(x/M_a, y/M_a)} \\ w'(x,y) &= circ(\rho) e^{i\varphi(x,y)} \end{aligned}, \qquad 3.6$$

where $\rho = \sqrt{x^2 + y^2}$ and $M_a = f_2 / f_1$ denotes the relative magnification of the pupils as the focal lengths of both lenses (L_1,L_2), figure 3.4, for this case the resultant vectorial beam amplitude of the Radial Shear-CSI entering the 4-f system is

$$\vec{t}_2(\rho) = \vec{J}_L\, w(\rho) + \vec{J}_R\, w'(\rho + \Delta\rho), \qquad 3.7$$

representing cross circular polarization states of the same beam radially sheared. As it was shown in the past section, in the image plane of the 4-f system the fringe pattern obtained is modulated by the Bessel function as Eq. 3.5 but presenting radial symmetry,

$$\begin{aligned} I_{q,r}(x_q, y_r) &= \left| P_{\psi_{q,r}}\, \vec{t}_0(x_q, y_r) \right|^2 = 2J_q^2 J_r^2 \left[1 + \cos\left(2\psi_{q,r} - \Delta\varphi(x_q, y_r)\right)\right] \\ \Delta\varphi(x_q, y_r) &= \varphi(x_q, y_r) - \varphi(x_q / M_a, y_r / M_a) \end{aligned} \qquad 3.8$$

where a translation of coordinates was used around the order position ($x_q = x - qF_0$ and $y_r = x - rF_0$), and $\Delta\varphi(x_q, y_r) = \varphi(x_q, y_r) - \varphi(x_q / M_a, y_r / M_a)$. In general, the interference pattern can be described as:[21]

$$I_i(x,y) = A(x,y) + B(x,y)\cos\left[2\psi_i - \frac{\partial\varphi(x,y)}{\partial x}\right] \qquad 3.9$$

for the case of lateral shear in x-direction. $I_i(x,y)$ represents the $i=1..4$ intensity distribution captured by the CCD camera in a single shot, the polarization filters angles are: $\psi_1=0°$, $\psi_2=45°$, $\psi_3=90°$ and $\psi_4=135°$, each of them represents phase shifts of $0°, 45°$, $90°$ and $135°$ respectively. By considering that $A(x,y)$ and $B(x,y)$ are constant the relative phase change can be calculated as:[34]

$$\frac{\partial\varphi(x,y)}{\partial x}=\arctan\left[\frac{I_1(x,y)-I_3(x,y)}{I_2(x,y)-I_4(x,y)}\right] \qquad 3.10$$

For the case of radial shear, Eq. 3.10 can be used only with the consideration of the radial dependency.

3.3 Cyclic Path Shearing Interferometer for Generation of Lateral and Radial Shear

Figure 3. shows the interferometers proposed for lateral shear and radial shear. The two optical systems are capable of obtaining in a single shot four shearograms with independent phase shifts. Figure 3.(a) shows the two possible interferometers that can be coupled to the 4-f system, each of them is used separately to generate a specified shear, the system-**I** is a Cyclic Shear Interferometer (CSI), where the shear is generated by moving the mirror M by a small distance Δs. The system-**II** is a cyclic radial shear interferometer (CRI), the optical setup is similar to the previously proposed, adding a pair of lens L_1 and L_2 to obtain the two beams with different diameter in the transversal section. In this case also lateral shear can be obtained only with a small displacement in *M*, resulting in a combination of a lateral and radial shear interferometer. Figure 3.2(b) shows the plots representing the superposition of amplitude spectra in the output of the two systems.

The system uses a He-Ne laser operating at $\lambda=632.8nm$. The collimated beam has a transversal section of $a=8.6mm$ and linear polarization state oriented to $45°\pm$ generated by a quarter-wave retarder (Q_0) and a linear polarizer (P_0). By the use of a polarizing beam splitter (PBS) the resulting beams have cross linear polarization and after passing the quarter wave retarder (Q_1), right and left circular polarization is obtained. The mirrors defined as M and M' are used to introduce the lateral shear Δs. The 4-f system coupled to the cyclic interferometer

uses two equals lenses (f =20 cm) and a phase grid defined as $G(\mu,\nu)$ placed in the posterior focal plane of the first lens. The system's pupil has a spatial period $d = \frac{1}{110} mm$. Replicated beams of the interference pattern are obtained from this configuration. Placing a linear polarizer on each replica, an independent phase-shift can be obtained. No extra corrections were used in the angle of the linear polarizers used because the quarter wave retarders (Q_0, Q_1) operate at the wavelength of the source.

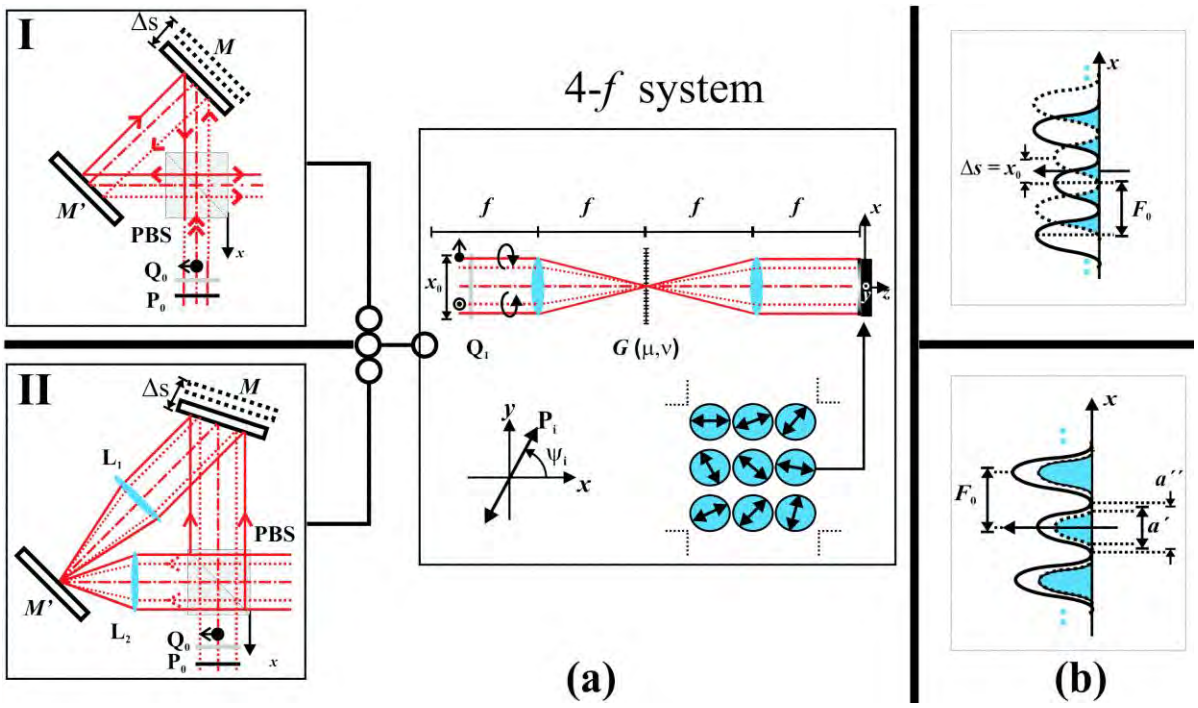

Figure 3.1 Cyclic Shearing interferometers with phase grid and modulation of polarization. (a) Configuration I is a variable lateral-shear interferometer were laterally sheared diffraction orders are superimpose (b-upper). Configuration II is a cyclic radial interferometer (CRI) were radially sheared diffraction order are superimpose (b-lower).

Lateral shear interferograms representing spherical aberration with defocusing are shown in Figure 3.. The Figure 3.(a) presents the four patterns obtained simultaneously with relative shifts of $\pi/2$. Phase derivative in x-direction is presented in Figure 3.(b). Figure 3.3 presents experimental results corresponding of an oil drop located on a microscope slide. The system may be used to measure the surface deformations in fluids and also measurement of the concentration gradients of liquids.

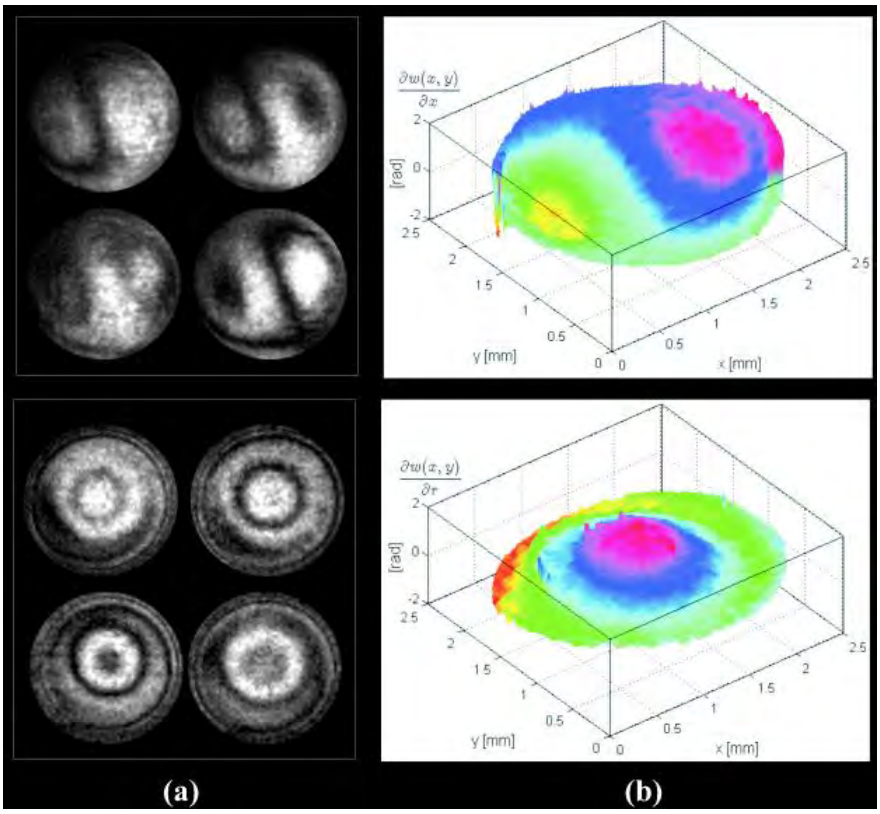

Figure 3.2 Experimental results corresponding of a lateral shear representing spherical aberration with defocusing.

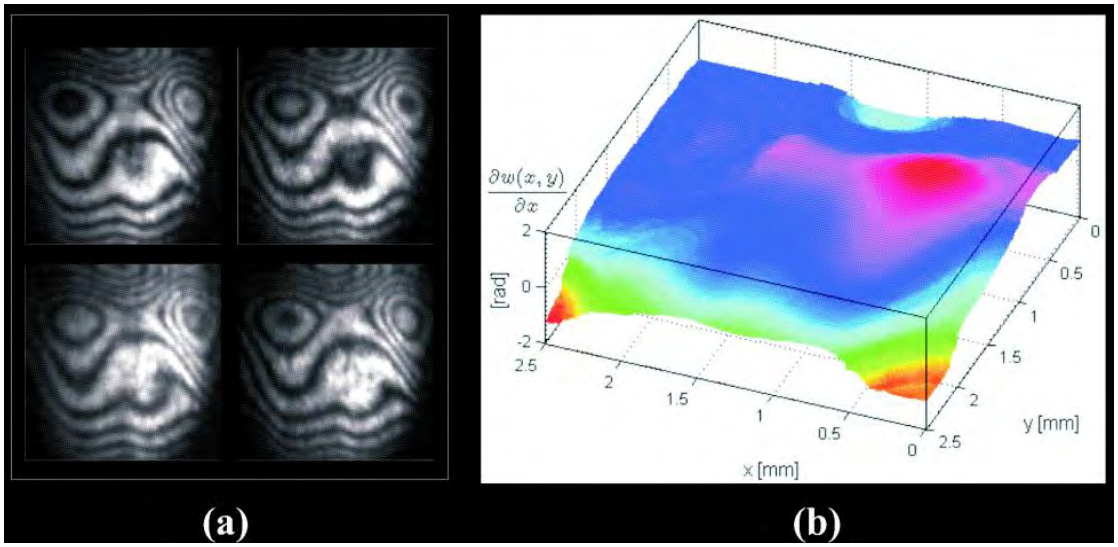

Figure 3.3 Experimental results corresponding of an oil drop located on a microscope slide.

3.4 Mach-Zehnder Radial Shear Interferometer

Figure 3. shows the experimental setup for radial slope measurements of transparent objects using a He–Ne laser operating at $\lambda = 632.8nm$. Linearly polarized light at 45° enters the interferometer using a quarter-wave retarder plate Q_0 and a linear polarizer P_0. The Mach–Zehnder radial-shear interferometer (MZRI), shown within a rectangle, is composed of two telescope systems (S_1, S_2) [21], one in each arm, in order to generate two radially sheared beams with slightly different magnifications at the output of the interferometer and with crossed lineal polarization (vertical and horizontal). A wave retarder plate of $\lambda/4$ (Q_1) is used to obtain cross circular polarization for each radial-shear wavefront (as before left and right, $\vec{J}_L$ and $\vec{J}_R$), which have equal intensity amplitude.

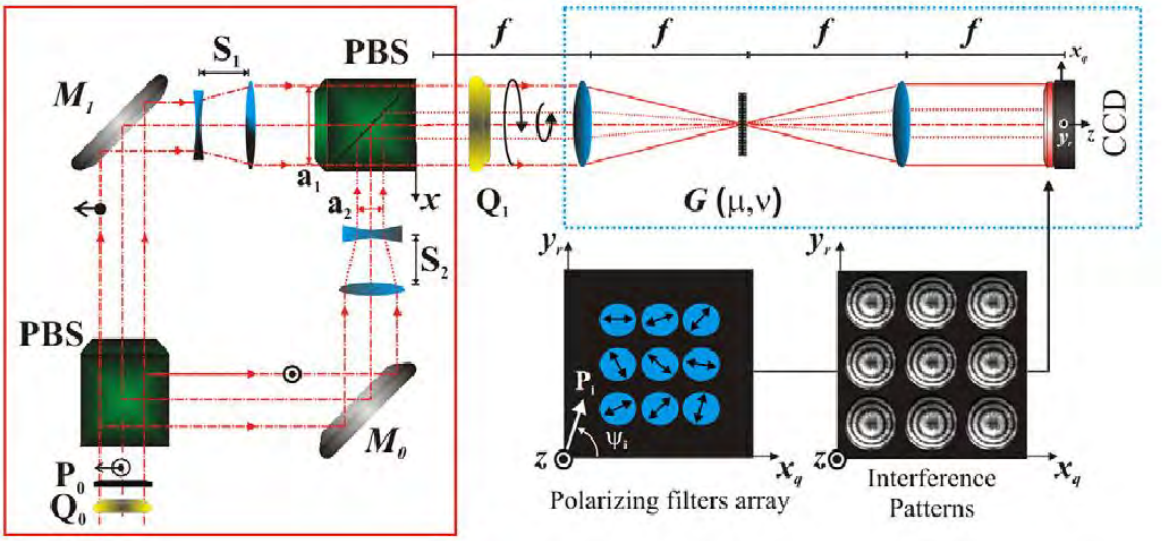

Figure 3.4 Radial Shearing interferometers with phase grid and modulation of polarization.

The 4-f system coupled to the cyclic interferometer uses two equals lenses (*f=20cm*) and a phase grid defined as $G(\mu,\nu)$ placed in the posterior focal plane of the first lens. A linearly polarized filter array is placed at the image plane, as presented in Figure 3.. Cross sections of the two sheared beams are $a_1 = 8.6mm$ and $a_2 = 7.0mm$, and the relative magnifications of the pupils is *M=1.23*.

Figure 3. shows experimental results for samples with radial symmetry and their associated radial slopes. Figure 3.(a) presents a characteristic radial-shear interference pattern obtained by interfering spherical wavefronts as a reference. The interference patterns obtained represent contours of constant radial slope, being symmetric about the center of curvature of the incident wavefront. Figure 3.(a) presents the radial slope with no sample and Figure 3.(b) shows the radial slope of an ophthalmic lens with a cross section of 5 *mm.*

Figure 3. shows the deformation caused by gravity in a lubricating oil drop placed over a microscope slide. The fringe pattern represents the stress field associated with the stabilization of the oil drop on the slide.

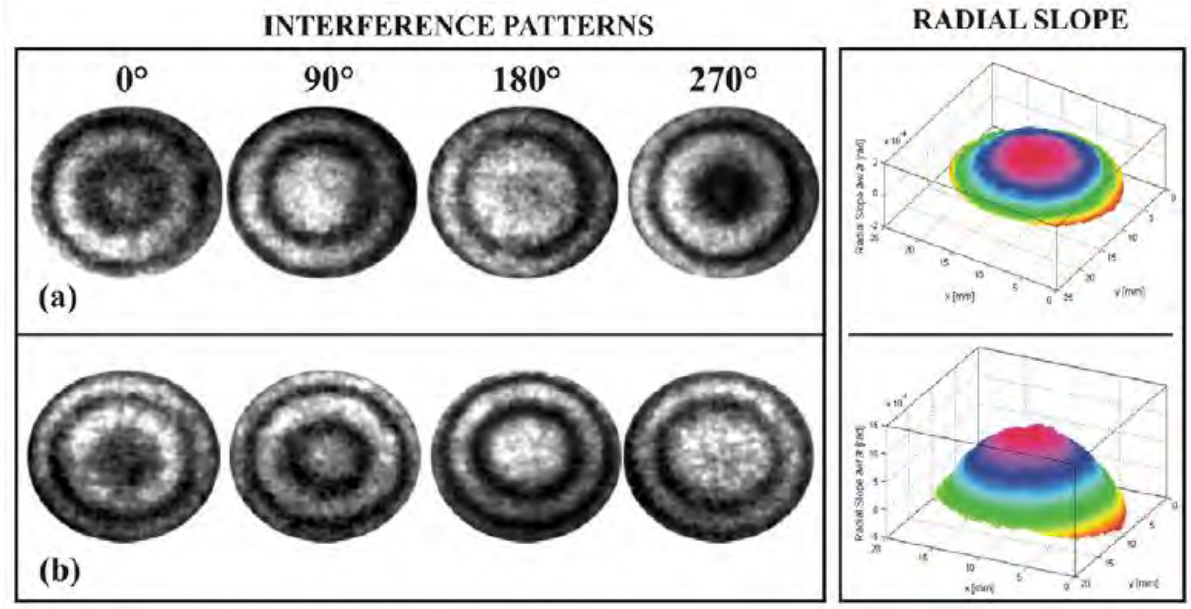

Figure 3.5 Experimental results for samples with radial symmetry and their associated radial slopes.

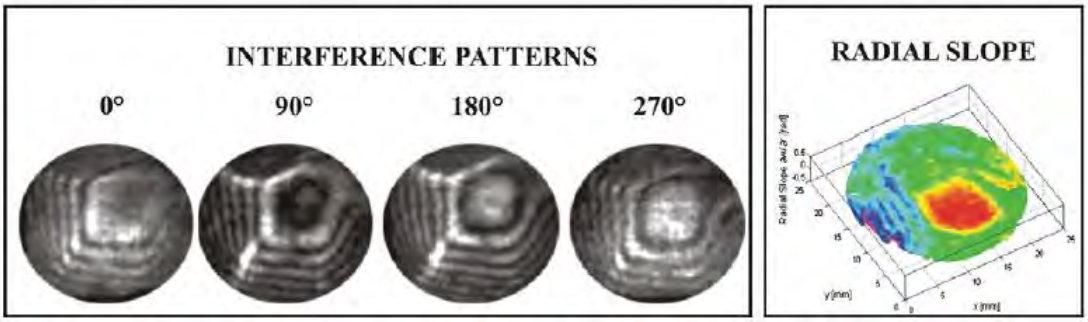

Figure 3.6 Lubricating oil that was placed on a microscope slide.

With the purpose of showing the capability of the optical system to study dynamic events (4D), we present results for lubricating oil that was placed on a microscope slide and then evaporated using a tin soldiering iron. The corresponding interferograms for successive captures of the CCD camera are shown in Figure 3., along with its associated radial slope

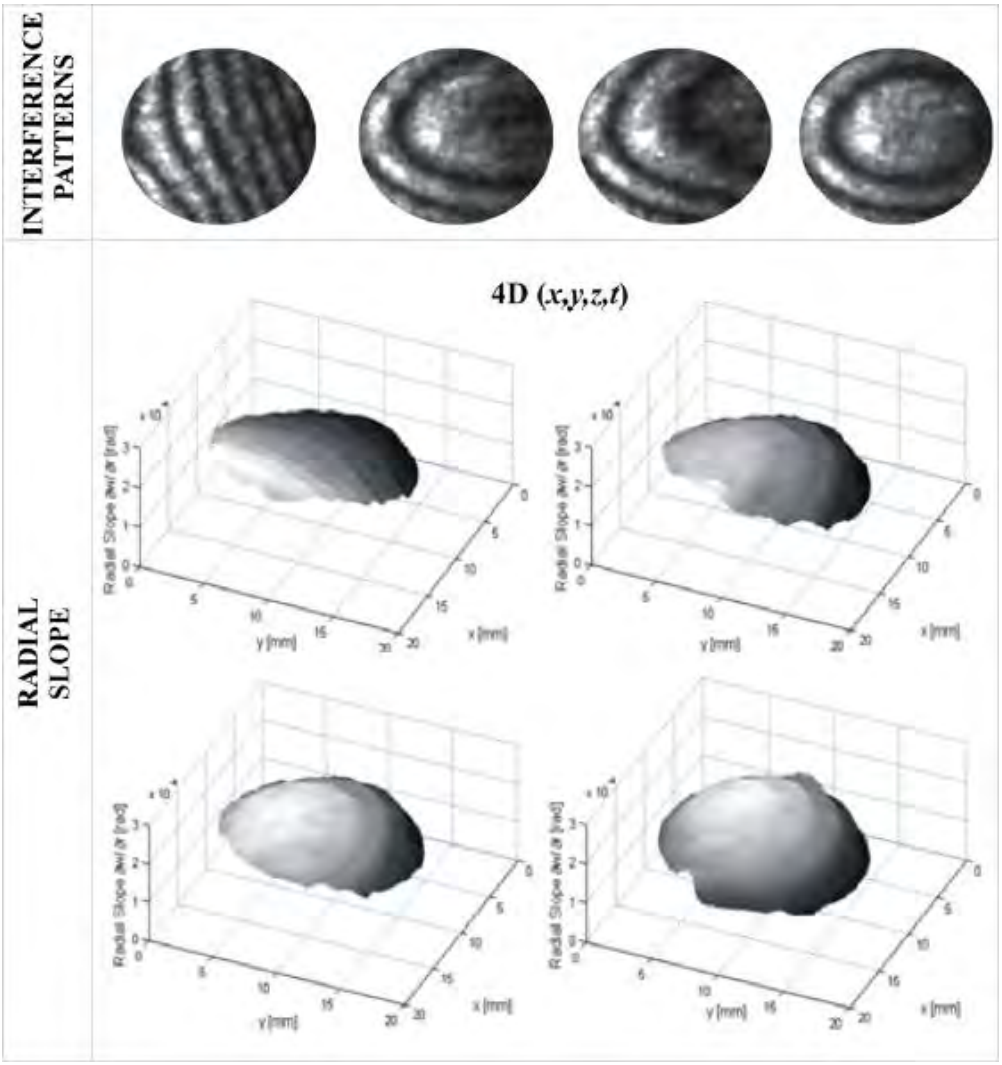

Figure 3.7 Lubricating oil that was placed on a microscope slide and then evaporated using a tin soldering iron.

3.5 Conclusion

Two systems were implemented: A cyclic shear interferometer and a Mach-Zehnder configuration. By adding a 4-f system with two crossed phase grating in the frequency plane, replicas of the output interferogram can be obtained. Each of these replicas can be freely phase shifted by polarization techniques. By selecting replication order with almost same amplitude intensity, a fringe pattern normalization algorithm can be avoided. The main issue to take into account is that the sample needs to be a phase sample.

Chapter 4

Dynamic Temperature Profile Measurements

In this chapter, an optical system capable of follow temperature field variations outside a thin-flame was implemented. The polarization phase shifting technique and a Michelson interferometer that is coupled to a 4-f system with a Ronchi grating placed at the frequency plane are used. This configuration permits to grab three phase-shifted interferograms simultaneously by one CCD. The temperature field measurement is based on measuring the refraction index difference by solving the inverse Abel transform, which requires information obtained by the fringe order localization. The phase map is retrieved by a three step algorithm. Experimental results of a dynamic thin flame are presented.

A quarter wave plate and a linear polarizer are positioned at the exit of an interferometer that has its reference and object beams with orthogonal linear polarization, a desired phase shift will be obtained and adjusted by the angle of the polarizer.[23,44] This consideration results suitable in the implementation for a single shift phase shifting interferometer.

The optical setup presented for the optical phase calculation is composed by a Polarization Michelson Interferometer (PMI) that is coupled to a 4-f system with an amplitude grating placed in the Fourier plane. As a result, the interferogram obtained firstly by the PMI is replicated in the image plane of the 4-*f* system.

Represented by the Jones calculation, the fields obtained by the reference and object beams in the PMI are described by $O(x,y)=\frac{1}{\sqrt{2}}\begin{pmatrix}1\\ i\end{pmatrix}e^{i\varphi(x,y)}$ and $R(x,y)=\frac{1}{\sqrt{2}}\begin{pmatrix}1\\ -i\end{pmatrix}$, representing left and right circular polarization states. The phase map $\varphi(x,y)$, represents the information to retrieve in a single capture. Later it is related to the temperature outside of the flame. When

each field is observed through a linear polarizing filter and made them interfere, the result is an interference pattern modulated by the angle ψ of the transmission axis of the linear polarizer.

By using an amplitude grating placed in the Fourier plane of the 4-*f* system, replicas of this interference pattern are obtained and recorded in the CCD. The major drawback of this system is the amplitude interferogram modulation obtained by the use of phase/amplitude gratings[21,45]. This information can be avoided by the implementation of fringe pattern normalization algorithms already encountered in the literature [46,47]. As a difference on the system presented previously in [19], in this work we only used a Ronchi ruling taking the interference replicas obtained in the $[-1,0,1]$ orders and use a fringe pattern normalization algorithm to avoid the interference amplitude difference against the $[-1,1]$ orders with the [0] order.

4.1 Temperature field measurement

The phase difference $\varphi(x,y)$ between two waves passing through the same point of the phase object, one in the presence of inhomogeneous medium and the other in the air, is given as[48–52]

$$\varphi(x,y)=\frac{2\pi}{\lambda}\int_0^{\Gamma}\left[n(x,y,z)-n_0\right]dz, \tag{4.1}$$

where $n(x,y,z)$ is the refractive index of the medium, n_0 the refractive index of the air and Γ is the total length of the medium. In Eq. 4.1 the optical path difference provides the distortion of the wavefront. In order to evaluate the index of refraction difference term, Eq. 4.1 must be inverted. This task can be achieved depending of the structure of the phase object. Taking the thin-flame as a phase object with radial symmetry, the equation of a bright fringe, $N(x)$, of the interferogram retrieved becomes[48]

$$N(x)\lambda=2\int_x^{\infty}\frac{f(r)rdr}{\sqrt{r^2-x^2}}, \tag{4.2}$$

where $f(r)=n(r)-n_0$. Eq. 4.2 represents the Abel transform of $f(r)$ and the index refraction difference is retrieved by using Abel transform inversion techniques[53,54]. By inverting Eq. 4.2, we are able to calculate the index of refraction profile dependent of the position. Taking into account the Gladstone-Dale relation, expressed under ideal gas assumption, we are able to retrieve the temperature profile as:

$$T(x,y)=\frac{P}{\left(\rho_{ref}+\frac{f(x,y)}{K_{G-D}}\right)R}, \tag{4.3}$$

taking air as a reference at T=15 °C with a pressure $P=101325\,N/m^2$, $\rho_{ref}=1.225kg/m^3$, $R=287\,J/kg\,K$ as the specific gas constant and $K_{G-D}=0.226\cdot10^{-3}m^3/Kg$ as the Gladstone-Dale constant at $\lambda=632.8nm$. Several studies concluded that the assumption of air is sufficient for premixed flames as a sample but in a more strictly manner the Gladstone-Dale and Specific gas constants need to be taken into account for specific local component distribution, not the scope of this work[55,56].

4.2 Experimental Setup

The proposed system is based on a PMI coupled to a 4-*f* system in order to obtain replicas of the interference pattern at the output, Figure 4.1. Using a He-Ne laser as a source, *λ=632.8 nm*, linearly polarized at 45° is divided in amplitude by the beam splitter (BS). In the object and reference arm of the PMI a linear polarizer at 0° and 90° is placed respectively, after the quarter-wave plate (QWP) located at 45° we are obtaining the interference of beams with circular polarization in opposite directions. If we placed a linear polarizer at this stage we could obtain an interference pattern with phase modulation controlled twice the linear polarizer angle. By placing an amplitude grating with spatial period of 100 *lines/mm* in the frequency plane of the 4-*f* system, we could obtain replicas with the same capability of phase modulation by placing a linear polarizer angle in each of the replicas obtained. As a result, we obtain the necessary interference fringe patterns with a relative phase shift in order to retrieve the phase data map properly. The monochromatic camera uses a CMOS sensor with 1280×1024 pixels and with a pixel pitch of *6.7μm*. The

polarizing filter film that was used is the commercially available. (Edmund Optics TechSpecs high contrast linear polarizing film). The size of each polarized film used in each interferogram was of 25x25mm with its transmission axis oriented at 0°, 60° and 120°. The wrapped phase data map was retrieved using the minimum least square algorithm of three steps[57] and the unwrapped phase data through the 2D Goldstein branch cut phase unwrapping algorithm[58].

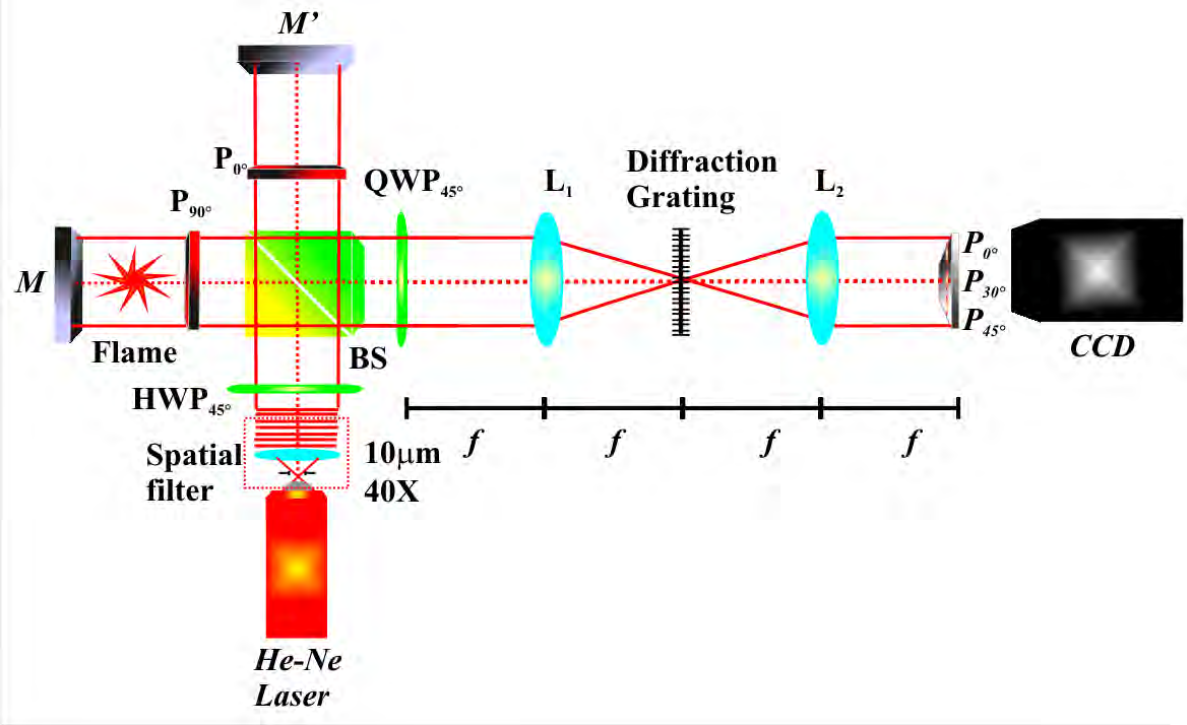

Figure 4.1 Setup of the instantaneous polarized phase-shifting interferometer. The Polarizing Michelson Interferometer (PMI) is coupled to a 4-f system in order to obtain replicas of the interference pattern at the output. Each interferogram retrieved presents a relative phase shift of 120°. Mirror: M; Half Wave Plate : HWP; Lens: Li; Polarizers: Pi; Quarter Wave Plate : QWP; Beam Splitter : BS.

Figure 4.2 presents the three phase shifted interferograms obtained by a single capture. After a previous calibration procedure[59] we are capable of retrieve the three phase shifted interference patterns. By implementing a fringe normalization technique we are capable of retrieve the phase data map, Figure 4.2(b). By taking a reference phase map the fringe order localization is directly obtained of the deformed fringe pattern, in this case caused by a thin-flame.

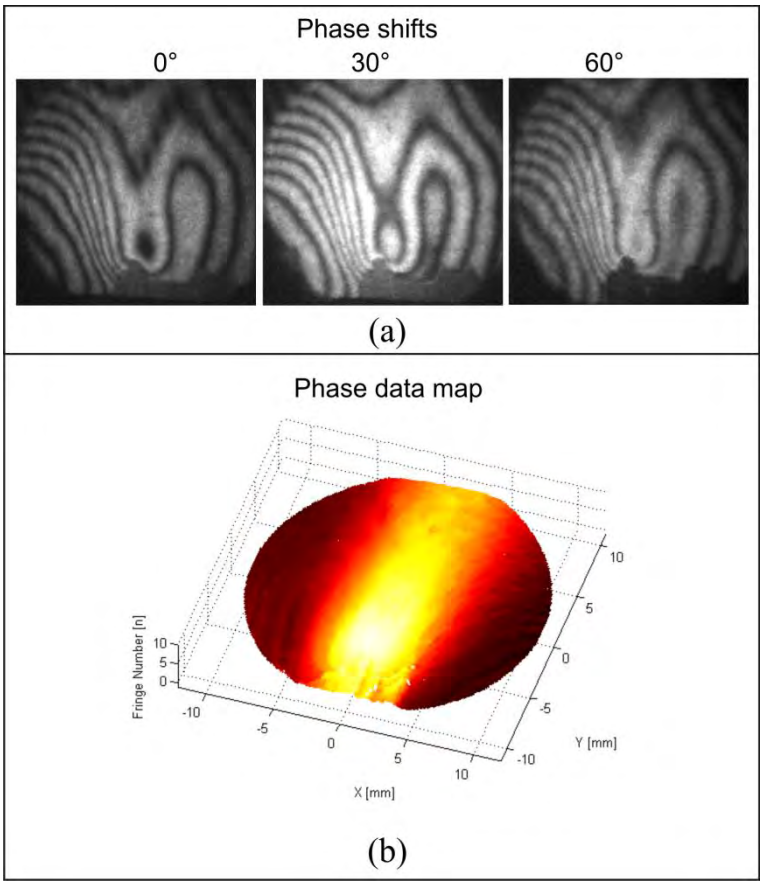

Figure 4.2 Experimental results correspondent to the fringe order number obtained by the unwrapped phase map. (a) Three phase shifted interferograms with amplitude modulation obtained by a single capture used to retrieve the phase data map. (b) By taking a reference phase map the fringe order localization is directly obtained from the deformed fringe pattern.

With the fringe order localization information we are capable of solve the inverse Abel transform, Eq. 4.2, and obtain the temperature change occurred by the thin-flame analyzed. Figure 4.3 shows the typical temperature profile obtained in a single capture. As the system is able to obtain the dynamic temperature profile, in Figure 4.4 we present several captures of a dynamic distribution of air temperature caused by ambient changes outside of the thin-flame.

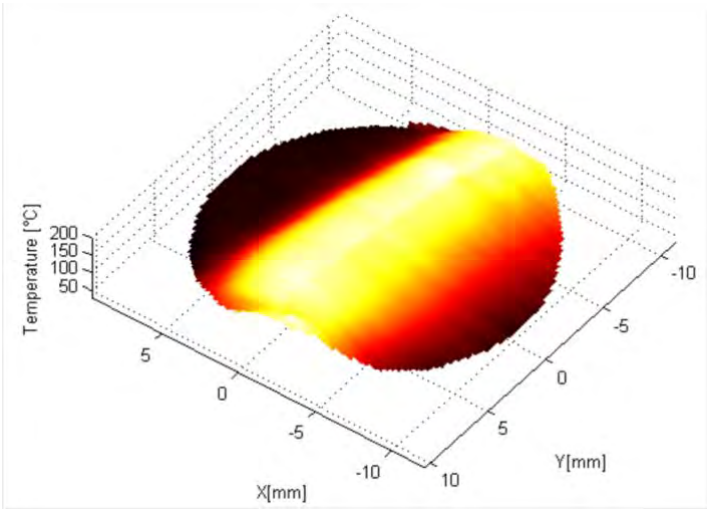

Figure 4.3 Temperature profile obtained in a single capture using polarizing phase shifting techniques.

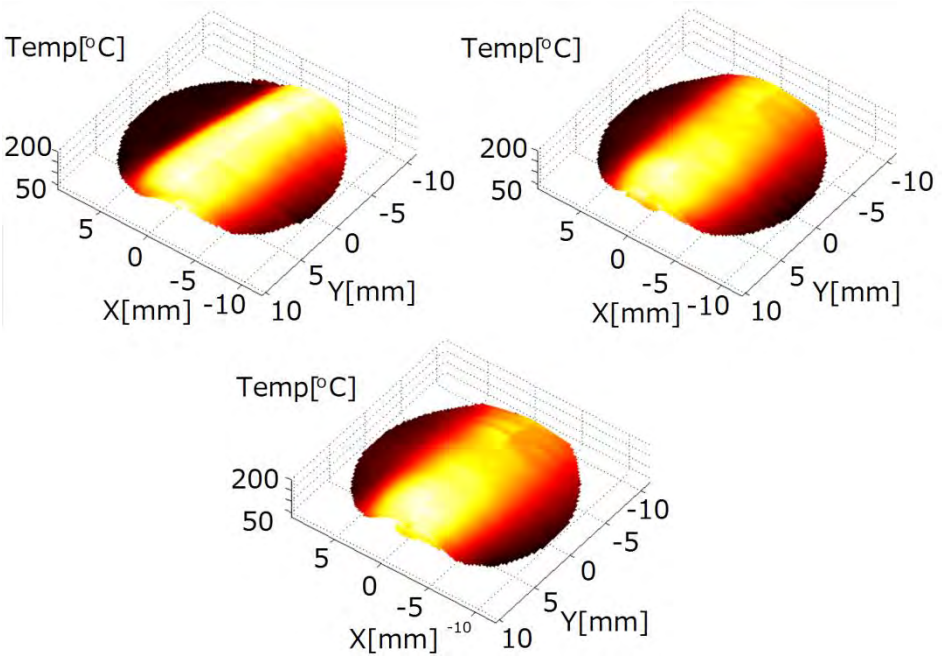

Figure 4.4 Temperature phase profiles varying in time (Representative frames).

4.3 Conclusion

The experimental setup for dynamic temperature field measurements using a single shot polarization phase shifting technique has been described. This system is able to obtain three phase shifted interferograms in only one shot. Therefore, it is suitable to carry out temporal measurements of temperatures changes occurring outside a thin-flame. The implementations of normalization fringe procedures present the advantage of avoiding the use of phase gratings and also the advantage of use only three interferograms for the analysis. The system is considerably simpler than previous proposals showing a suitable alternative to implements in an industrial ambient.

Chapter 5

Single Shot Phase Shifting Interferometry using a Two-Interferograms Phase Shifting Algorithm

A Polarization Mach Zehnder Interferometer (PMZI) was implemented to analyze transparent samples using a two-step algorithm to retrieve optical phase data. The major drawback of the two-step phase shifting algorithms is that it can't be used when the phase shift is π; this case arises when using a polarizing beam splitter as a detector when interfering cross circular polarized beams. In order to take advantage of the PMZI, the beams have to meet certain conditions to properly obtain the interference patterns and correctly retrieve the optical phase data. We present the analytical model of the conditions and experimental results for a static event. The configuration presented does not require micro-polarizer arrays or the use of conventional polarizing filters to yield a phase shift, resulting in an increase in the intensity and resolution of the measurements.

The most important and an industry standard nowadays are the pixelated phase mask interferometers but one of the limitations of these systems is that the modulating phase-mask remains fixed. By the use of phase/amplitude-gratings, more than four phase shifted interferograms can be acquired in a single capture, but in some cases a certain fringe normalization procedure needs to be applied to the interferograms.[46] The purpose of this research is to propose an alternative system using out of the shelf polarizing components and also extend the use of these two current systems, gratings or pixelated phase cameras, by following the polarizing properties of the system by the procedure presented.

5.1 Polarization Phase Shifting using Two-Interferograms

Figure 5.1 presents the experimental setup used based on a Polarization Mach-Zehnder Interferometer (MZI) with the addition of two Quarter Wave Plates (QWP) in a rotatory stage placed one in each arm of the PMZI. The main purpose of this work is to control the relative phase shift between two interferograms by finding the proper values of the QWP angles.

By describing the polarization states of each beam, in the interferometer, while they go through each polarization component of the MZI, we could obtain the interferograms equations as

$$I_{1,2}(x,y) = A_{1,2}(x,y) + B_{1,2}(x,y)Sin\left[\varphi(x,y) + C_{1,2}(x,y)\right], \tag{5.1}$$

where $\varphi(x,y)$ is the phase map to be retrieved, $A_{1,2}(x,y)$ represents the bias term of the interferogram, obtained as

$$\begin{aligned} A_1(x,y) &= \frac{1}{4}\left[3 + Cos(4\theta_1) + Cos(4\theta_2)\right] \\ A_2(x,y) &= \frac{1}{8}\left[2 - Cos(4\theta_1) + Cos(4\theta_2)\right]. \end{aligned} \tag{5.2}$$

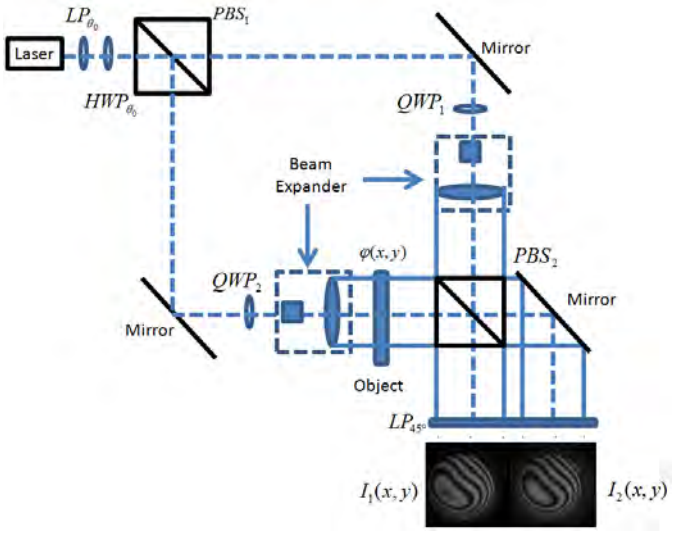

Figure 5.1 Mach-Zehnder Interferometer used to obtain two-phase shifted with a relative phase shift different from π. P*BS*: Polarizing Beam-Splitter, *LP*: Linear Polarizer, *QWP:*Quarter wave-plate. *M:* Mirror.

$B_{1,2}(x,y)$ represents the amplitude modulation term of the interferogram obtained as

$$B_1(x,y)=\frac{1}{2}\left[3+\frac{3}{2}Cos(4\theta_1)+\frac{3}{2}Cos(4\theta_2)+Cos(4\theta_1)Cos(4\theta_2)\right]^{1/2}$$
$$B_2(x,y)=-\frac{1}{2}Sin(2\theta_1)Sin(2\theta_2) \qquad 5.3$$

and $C_{1,2}(x,y)$, the phase shift in each of the interferogram, as

$$C_1(x,y)=Tan^{-1}\left(\frac{-1+Cos(2\theta_1)Cos(2\theta_2)}{Cos(2\theta_2)+Cos(2\theta_1)}\right)$$
$$C_2(x,y)=-\pi/2 \qquad 5.4$$

By having separated each part of the interferograms, we could represent them in a 3D space. The [x,y] axis represents the angular value $[\theta_1,\theta_2]$of each $QWP_{1,2}$ and the z axis denotes the relative change between each term (bias, amplitude and phase shift term). Figure 5.2 presents the relative difference between the interferograms for each term.

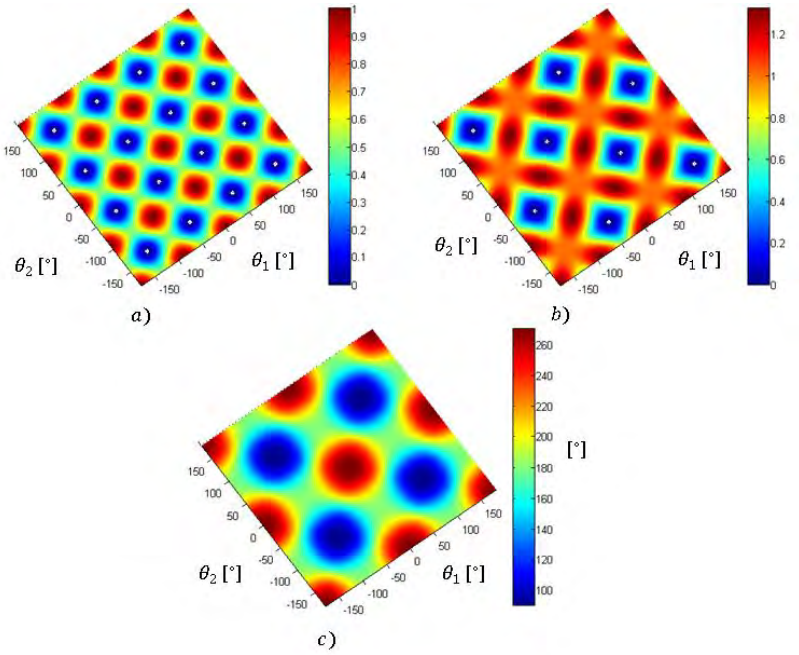

Figure 5.2 Relative difference of the interferograms terms. a) Bias Term, b) Amplitude Modulation Term and the c) Phase Shift depending on the angles of the QWP located on each arm of the MZI.

With the diagram of each interferogram terms, we are able to obtain the regions where the bias and amplitude modulation term, for both interferograms, are almost equal. The final purpose is to obtain the permitted relative phase shift between the interferograms, Figure 5.3. In this case we needed to obtain interferograms with a relative phase shift different from 180º as the phase demodulation algorithm demands.

5.2 Experimental Results

Figure 5.4 presents experimental results corresponding of a misaligned to misalignments of one of the beam expanders of the object beam. The two interferograms are captured in a single image by the CCD camera, processed by a fringe pattern normalization algorithm and out of this the phase demodulation term is found by a two-step demodulation algorithm.[60,61] To unwrap the phase map, the 2D Goldstein branch cut algorithm is used.[58] The angles selected for this experiment are $\theta_1 = -50^o$ and $\theta_2 = 50^o$, corresponding to a relative phase shift of 160 º

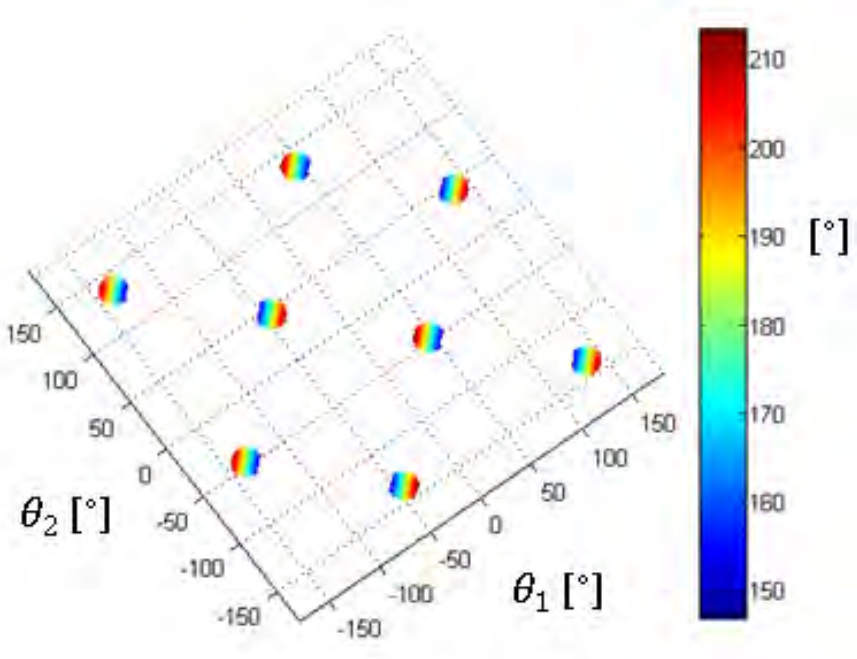

Figure 5.3 Permitted QWP angles, $[\theta_1, \theta_2]$, were the amplitude and the modulation terms remain unchanged. This in order to obtain a relative phase shift different from 180° as the phase demodulation algorithm requires.

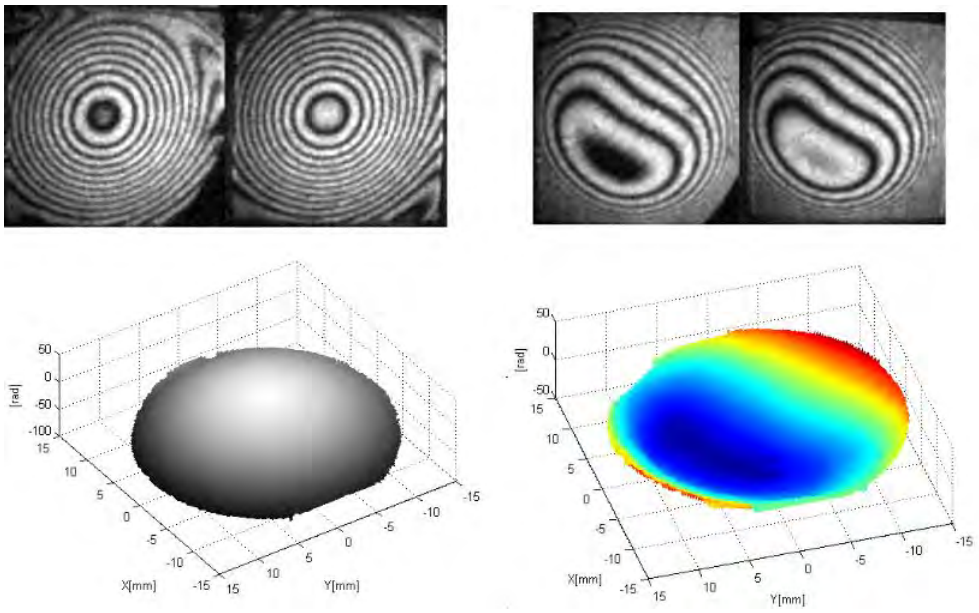

Figure 5.4 Experimental results obtained by misalignment of one of the collimating lens in the beam expander.

5.3 Conclusion

We presented a single shot phase shifting interferometer based on polarization phase shifting techniques. The major novelty of the present system is to avoid the use of special components to replicate the beam as a pixelated phase mask or amplitude/phase gratings. The final purpose of this work is to develop a platform dedicated to describe the phase change in real time.

Chapter 6

Dynamic birefringence mapping by a polarization image sensor

In order to expand the implementation of single shot phase shifting techniques, one part of the Phd Project was focused on learning and developing knowledge related to birefringence mapping. This chapter comprises some of the topics developed in a research internship in the Center for Optical Research and Education (CORE).

In recent years, dynamic measurement of birefringence distribution has been required to analyze internal stress structures of materials, and macromolecule flow or orientation of functional polymer materials. Some commercial systems for a birefringence measurement have been proposed, but there are limitations for getting higher speed phenomenon because of the phase modulation. The birefringence distribution and azimuth angle direction can be analyzed using single shot phase shifting techniques by using the Mueller matrix and Stokes parameters.[62,63]

For two-dimensional birefringent measurements, a phase-shifting technique has been developed before using a half-wave plate and a Babinet-Soleil compensator as phase shifters,[62] by using the replication method of the pixelated phase camera a single shot birefringence measurement can be implemented.

The optical setup used in this study is shown in Figure 6.1. This setup consists of a monochromatic light source, a polarizer, a quarter-wave plate, a birefringent specimen, and the CCD camera with a microretarder array. Light passes through the polarizer whose optical axis is horizontal, and through a quarter-wave plate whose fast axis makes an angle of 45 deg with respect to the *x* axis. Then, the circularly polarized light passes through the birefringent

specimen. The light emerging from the birefringent specimen is acquired by the polarization-imaging camera.

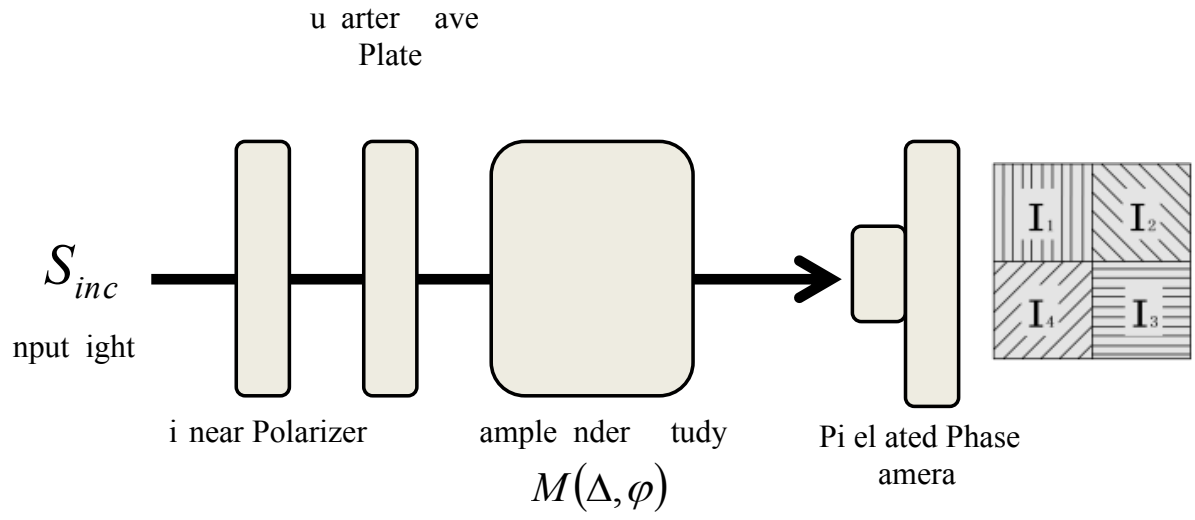

Figure 6.1 Optical setup dedicated to obtain birefringence measurements of a sample using a pixelated phase camera as a detector.

By employing the Mueller Matrix approach, the Stokes vector of the light beam emerging from the specimen can be written as

$$S_{out} = \begin{bmatrix} S_{out\_1} \\ S_{out\_2} \\ S_{out\_3} \\ S_{out\_4} \end{bmatrix} = LP_{\theta} M_{\Delta,\varphi} QWP_{45} LP_0 S_{inc}, \tag{6.1}$$

where S_{inc} is the input incident light represented by

$$S_{inc} = \begin{bmatrix} S_{inc\_1} \\ S_{inc\_2} \\ S_{inc\_3} \\ S_{inc\_4} \end{bmatrix}. \tag{6.2}$$

where S_{inc_1} represents the total intensity of the beam, S_{inc_2} the intensity related for linear horizontal/vertical polarization state, S_{inc_3} the intensity part with linear polarization state at

$\pm 45°$ and S_{inc_4} the contribution of the light with circular polarization state. The matrix for the linear polarizer LP_θ at θ,[64,65]

$$LP_\theta = \frac{1}{2}\begin{bmatrix} 1 & \cos 2\theta & \sin 2\theta & 0 \\ \cos 2\theta & \cos^2 2\theta & \sin 2\theta \cos 2\theta & 0 \\ \sin 2\theta & \sin 2\theta \cos 2\theta & \sin^2 2\theta & 0 \\ 0 & 0 & 0 & 0 \end{bmatrix}, \tag{6.3}$$

a quarter wave plate at 45 degrees,

$$QWP_{45} = \begin{bmatrix} 1 & 0 & 0 & 0 \\ 0 & 0 & 0 & -1 \\ 0 & 0 & 1 & 0 \\ 0 & 1 & 0 & 0 \end{bmatrix}, \tag{6.4}$$

and the sample under study $M_{\Delta,\varphi}$ with phase difference and principal optical axis direction is:

$$M_{\Delta,\varphi} = \begin{bmatrix} 1 & 0 & 0 & 0 \\ 0 & 1-(1-\cos\Delta)\sin^2 2\varphi & (1-\cos\Delta)\sin 2\varphi \cos 2\varphi & -\sin\Delta \sin 2\varphi \\ 0 & (1-\cos\Delta)\sin 2\varphi \cos 2\varphi & 1-(1-\cos\Delta)\cos^2 2\varphi & \sin\Delta \cos 2\varphi \\ 0 & -\sin\Delta \sin 2\varphi & -\sin\Delta \cos 2\varphi & \cos\Delta \end{bmatrix}. \tag{6.5}$$

By making the corresponding matrix multiplication, the detected intensity is obtained by taking the first element of the output state (S_{out_1}).

$$I_\theta = S_{out\_1} = \frac{1}{2} I_0 \left[1 - \sin\Delta \sin(2\theta - 2\varphi)\right] \tag{6.6}$$

Suppose the light intensity is I_1, I_2, I_3, and I_4 when the direction θ of the analyzer is 0°, 45°, 90°, and 135°, respectively. Applying the phase-shifting method, the incident light intensity I_0,

$$I_0 = \frac{I_1 + I_2 + I_3 + I_4}{2}, \tag{6.7}$$

the principal a is direction φ,

$$\varphi = \frac{1}{2}\tan^{-1}\frac{(I_3 - I_1)}{(I_2 - I_4)} \tag{6.8}$$

and the phase difference Δ can be e pressed as [63]

$$\Delta = \sin^{-1} \frac{\sqrt{(I_3 - I_1)^2 + (I_2 - I_4)^2}}{I_0}. \qquad 6.9$$

6.1 Experimental Results

A two-dimensional birefringence distribution measurement system with a sampling rate of 1.3 MHz was used[66]. The polarization image sensor was composed of a pixelated polarizer array made from photonic crystal[67] and a parallel read out circuit with a multi-channel analog to digital converter specialized for two-dimensional polarization detection[66]. By applying phase shifting algorism with circularly-polarized incident light, birefringence phase difference Δ and azimuthal angle φ can be measured. Figure 6.2 presents experimental results of an epoxy transparent sample under compression. The phase difference Δ term (related with the fringe contrast term) represents the information about the retardance change due to the compression; the azimuthal angle φ term is directly related with the fast angle axis.

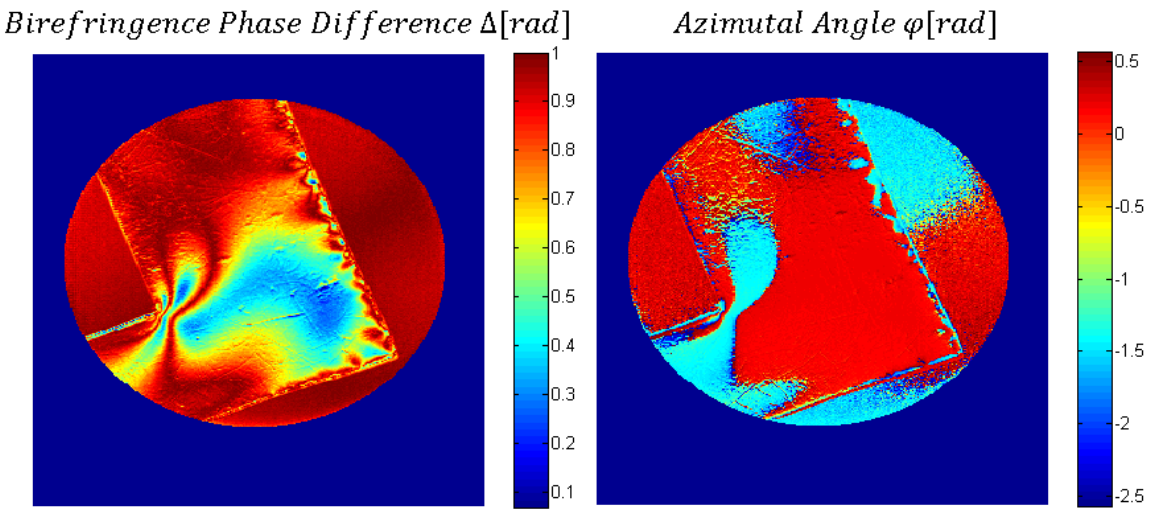

Figure 6.2 Experimental results of an epoxy transparent sample under compression.

By setting the polarization imaging camera at *1000 fps* we were able to retrieve an image of 1024x1024 pixels, the compression of the epoxy sample changing in time was followed. Representative frames are presented in Figure 6.3. Another experimental result is the follow of the compression occurred in an acrylic block hitted by a hammer, in this case the polarization camera was set at *10,000 fps*, Figure 6.4 presents representatives figures of the event.

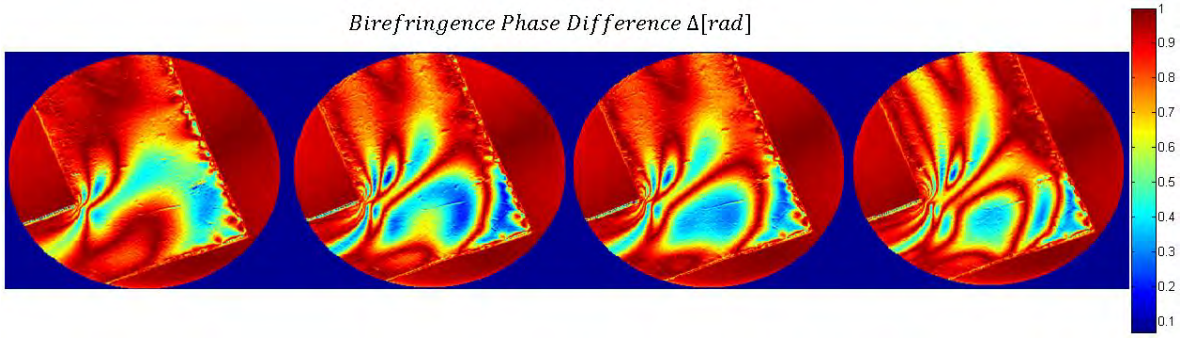

Figure 6.3 Temporal evolution of the epoxy transparent sample under compression by observing the birefringence distribution varying in time.

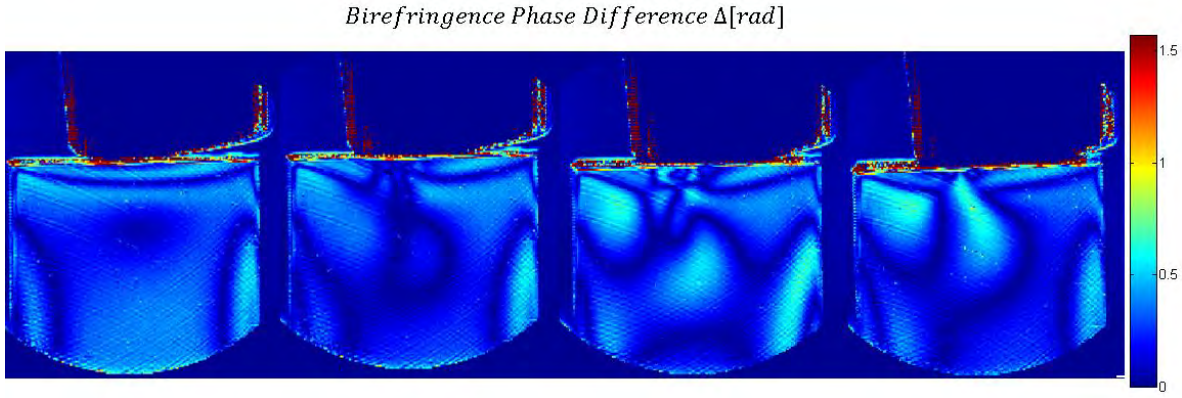

Figure 6.4 Temporal evolution of an acrylic block hit by a hammer at *10,000 fps*.

6.2 Conclusion

A birefringence imaging system composed by a high speed pixelated camera was presented. The system tested is capable of following dynamic phase changes at speeds of up to 10,000 fps. Although the measurement system is based on purely polarization properties of the sample, this research field can be associated with the work done in interferometry measurements by taking into account that the information is carried on the amplitude modulation change of the interferogram.

Conclusions and Future Work

This thesis explored the concept of polarization phase shifting techniques, focusing particularly on implementation of single shot phase interferometers based on a 4-f system. Polarization phase shifting techniques requires several conditions that need to be met in order to be implemented, the most important is that the reference and object beams have orthogonal polarization states. By using the 4-f system with gratings placed on the frequency plane, an amplitude modulation is produced on the image plane in each of the replica obtained. This can be dealt by using normalization procedures or by using replicas orders with almost the same amplitudes.

Several single shot phase shifting interferometry techniques were successfully implemented to analyze phase changes varying in time. The approach developed in this thesis has served to propose new interferometric systems, as the common path configuration based on grating interferometry techniques. Different types of measurements have been done, such as slope phase measurements and temperature profiles. The proposed systems consider the geometric and polarization properties of the interferometer. Table 1 presents advantages and disadvantages of the systems implemented.

The common path interferometer, based in grating interferometry techniques, takes into account the intrinsic π-phase shifted replicated interferograms obtained to reduce the number of linear polarizer placed at the output, the system have the limitations of the size of the lens and the quarter wave plates used.

The slope phase measurement system presented have the property of obtain more interferograms to process the phase, opening possibilities to use different phase processing algorithms. One of the disadvantages of this system is that by increasing the number of replicas a reduction of the spatial resolution is encountered.

A system capable of measuring temperature profiles was implemented. The system uses only three interferograms for the analysis. A disadvantage presented is the fringe

normalization process to compensate the amplitude change due to the replication method used. This system is simpler than the previous proposed showing a suitable option for industrial environments applications.

A system were proposed with the principal characteristic of process the phase by using a two-interferogram algorithm and avoiding the usage of the 4-f system as the replication method. The phase shift was controlled by polarization properties of the reference and object beams.

A 2D birefringence mapping system was implemented. The system is based in treat the sample as a linear retarder. By taking into account properties related with the phase shifting algorithms, the information is encoded in the phase and its amplitude modulation.

One of the main limitations common in the implemented systems is that the samples need to maintain the polarization properties of the beam, and that they have to be phase sample. As a future work, considerations based on the Mueller matrix approach of the sample can be used as a compensation of this. Another future work is to use the pixelated camera as a calibration system of a polarization interferometer.

Single Shot Phase Shifting Interferometry Based in Polarization Techniques		
System	*Advantages*	*Disadvantages*
Quasi-Common Path Interferometer	• Insensibility of external vibration due to of the common path characteristic. • Reduction of the numbers of the linear polarizer mask due to of the π-shift intrinsically obtained.	• Reduction of the spatial resolution. • Field of view highly dependent of the light source, lens and period of the grating used.
Slope Phase Measurements	• Obtain more than 4 interferograms. • Sample placed outside of the interferometer. • Slope of the phase change obtained directly.	• Reduction of the spatial resolution. • Phase information obtained through an integration process.
Temperature Profile Measurements	• Three interferograms to process the phase.	• Temperature is obtained by projected lines. • Polarization state of the object beam may be affected by the sample. • Contrast changes compensated by a fringe pattern normalization algorithm.
Two-Interferograms Phase Shifting Interferometer	• Avoid the usage of the 4-f system. • Two interferograms to process the phase.	• Phase algorithm demands a phase shift different from π. • Contrast changes compensated by a fringe pattern normalization algorithm.
2D Birefringence Mapping	• High speed measurement capability.	• Sample is treated as a pure linear retarder. • Birefringence measurement range of $\pi/2$. It goes from 0 to $\pi/2$

Table 1 – Advantages and disadvantages of the implemented systems.

References

1. Yamaguchi, ., Kato, J., Ohta, . & Mizuno, J. “Image formation in phase-shifting digital holography and applications to microscopy.” *Applied Optics* **40,** 6177–6186 (2001).

2. Gorthi, . . & Rastogi, P. “Fringe projection techniques: hither we are?” *Optics and Lasers in Engineering* **48,** 133–140 (2010).

3. Martínez, A., Rayas, J. A., Puga, H. J. & Genovese, K. “ terative estimation of the topography measurement by fringe-projection method with divergent illumination by considering the pitch variation along the and z directions.” *Optics and Lasers in Engineering* **48,** 877–881 (2010).

4. Liu, J.-P. & Poon, T.- . “Two-step-only quadrature phase-shifting digital holography.” *Optics Letters* **34,** 250–252 (2009).

5. Nakadate, . “Vibration measurement using phase-shifting speckle-pattern interferometry.” *Applied Optics* **25,** 4162 (1986).

6. Griffin, D. . “Phase-shifting shearing interferometer.” *Optics Letters* **26,** 140–141 (2001).

7. Kothiyal, M. P. & Delisle, . “ hearing interferometer for phase shifting interferometry with polarization phase shifter.” *Applied Optics* **24,** 4439 (1985).

8. Serrano-García, D. I., Toto-Arellano, N. I., Martínez-Garcia, A., Rayas-Álvarez, J. A., Téllez-Quiñones, A. & Rodríguez-Zurita, G. “ imultaneous phase-shifting cyclic interferometer for generation of lateral and radial shear.” *Revista Mexicana de Física* **57,** 255–258 (2011).

9. Novak M., Millerd J., Brock N., North-Morris M., Hayes J., . J. “Analysis of a micropolarizer array-based simultaneous phase-shifting interferometer.” *Applied Optics* **44,** 6861–6868 (2005).

10. Neal, R. M. & Wyant, J. . “Polarization phase-shifting point-diffraction interferometer.” *Applied Optics* **45,** 3463–3476 (2006).

11. Rodriguez-Zurita, G., Toto-Arellano, N.-I., Meneses-Fabian, C. & Vázquez-Castillo, J. F. “One-shot phase-shifting interferometry: five, seven, and nine interferograms.” *Optics Letters* **33,** 2788–2790 (2008).

12. Baker, K. . & tappaerts, E. A. “A single-shot pixellated phase-shifting interferometer utilizing a liquid-crystal spatial light modulator.” *Optics Letters* **31,** 733–735 (2006).

13. Wyant, J. . “Vibration insensitive interferometric optical testing - OSA Technical Digest (D) .” in *Frontiers in Optics 2004/Laser Science XXII/Diffractive Optics and Micro-Optics/Optical Fabrication and Testing* OTuB2 (Optical Society of America, 2004). at <http://www.opticsinfobase.org/abstract.cfm?URI=OFT-2004-OTuB2>

14. Chen, L.-C., Yeh, S.-L., Tapilouw, A. M. & Chang, J.- . “3-D surface profilometry using simultaneous phase-shifting interferometry.” *Optics Communications* **283,** 3376–3382 (2010).

15. Millerd, J., Brock, N., Hayes, J., North-Morris, M., Kimbrough, B. & Wyant, J. C. in *Fringe 2005* 640–647 (2006). doi:10.1007/3-540-29303-5_86

16. ervin, M. & Estrada, J. . “Error-free demodulation of pixelated carrier frequency interferograms.” *Optics Express* **18,** 18492–18497 (2010).

17. Padilla, J. M., ervin, M. & Estrada, J. . “ ynchronous phase-demodulation and harmonic rejection of 9-step pi elated dynamic interferograms.” *Optics Express* **20,** 11734 (2012).

18. Brock, N., Millerd, J., yant, J. & Hayes, J. “Pi elated phase-mask interferometer.” (2005). at <http://www.google.com.tr/patents/US20050046865>

19. Toto-Arellano, N.-I., Martínez-García, A., Rodríguez-Zurita, G., Rayas-Álvarez, J. A. & Montes-Perez, A. “ lope measurement of a phase object using a polarizing phase-shifting high-frequency Ronchi grating interferometer.” *Applied optics* **49,** 6402–6408 (2010).

20. Toto-Arellano, N.-I., Rodriguez-Zurita, G., Meneses-Fabian, C. & Vazquez-Castillo, J. F. “Phase shifts in the Fourier spectra of phase gratings and phase grids: an application for one-shot phase-shifting interferometry.” *Optics Express* **16,** 19330–19341 (2008).

21. Serrano-García, D. I., Toto-Arellano, N.-I., Martínez-García, A. & Zurita, G. R. “Radial slope measurement of dynamic transparent samples.” *Journal of Optics* **14,** 045706 (2012).

22. yant, J. . “ ourse Notes - Optics 513 - hapter 5.” at <http://fp.optics.arizona.edu/jcwyant/Optics513/ChapterNotes/Chapter05/Notes/Geometric_Phase_Shifter.pdf>

23. Bryngdahl, O. “Polarization-Type Interference-Fringe hifter.” *Journal of the Optical Society of America* **62,** 462 (1972).

24. Hariharan, P. “Achromatic phase-shifting for white-light interferometry.” *Applied Optics* **35,** 6823–6824 (1996).

25. Helen, . ., Kothiyal, M. P. & irohi, R. . “Achromatic phase shifting by a rotating polarizer.” *Optics Communications* **154,** 249–254 (1998).

26. hagam, R. N. & yant, J. . “Optical frequency shifter for heterodyne interferometers using multiple rotating polarization retarders.” *Applied Optics* **17,** 3034–5 (1978).

27. “Edmund Optics - Precision Ronchi Ruling Glass lides.” at <http://www.edmundoptics.com/testing-targets/test-targets/resolution-test-targets/precision-ronchi-ruling-glass-slides/1831?ref=related-products>

28. “Edmund Optics - Transmission Grating Beamsplitters.” at <http://www.edmundoptics.com/optics/gratings/transmission-grating-beamsplitters/1939>

29. Toto-Arellano, N.-I., Rodríguez-Zurita, G., Martínez García, A., Vázquez-Castillo, J. F. & Rayas Álvarez, J. A. “Analysis of the Pi phase-shifts obtained in the Fourier spectra of phase gratings and grids by using two-window grating interferometry.” *Revista mexicana de Física* **56,** 281–286 (2010).

30. Goodman, J. . “ ntroduction to Fourier Optics McGraw-Hill Series in Electrical and omputer Engineering.” *Quantum and Semiclassical Optics Journal of the European Optical Society Part B* **8,** 491 (1996).

31. Serrano-García, D. I., Toto-Arellano, N.-I., Martínez-García, A. & Zurita, G. R. “Radial slope measurement of dynamic transparent samples.” *Journal of Optics* **14,** 45706 (2012).

32. Serrano-García, D. I., Martínez-García, A., Rayas-Alvarez, J. A., Toto-Arellano, N. I., Rodriguez-Zurita, G. & Montes-Pérez, A. “Adjustable-window grating interferometer based on a Mach-Zehnder configuration for phase profile measurements of transparent samples.” *Optical Engineering* **51,** 055601 (2012).

33. Rodriguez-Zurita, G., Meneses-Fabian, C., Toto-Arellano, N.-I., Vázquez-Castillo, J. F. & Robledo- ánchez, . "One-shot phase-shifting phase-grating interferometry with modulation of polarization: case of four interferograms." *Optics Express* **16,** 7806–7817 (2008).

34. Malacara, D., Servín, M. & Malacara, Z. "*Interferogram Analysis For Optical Testing,*". *Interferogram Analysis For Optical Testing, Second Edition* 440 (2005). doi:doi:10.1201/9781420027273.fmatt

35. Rodriguez-Zurita, G., Meneses-Fabian, C., Toto-Arellano, N.-I., Vázquez-Castillo, J. F. & Robledo- ánchez, . "One-shot phase-shifting phase-grating interferometry with modulation of polarization: case of four interferograms." *Optics Express* **16,** 7806 (2008).

36. Kemao, ., Xiaoping, . & Asundi, A. "Grating-Based Real-Time Polarization Phase- hifting nterferometry: Error Analysis." *Applied Optics* **41,** 2448 (2002).

37. Toto-Arellano, N. I., Rodriguez-Zurita, G., Meneses-Fabian, C. & Vázquez-Castillo, J. F. "A single-shot phase-shifting radial-shearing interferometer." *Journal of Optics A: Pure and Applied Optics* **11,** 45704 (2009).

38. Rodríguez-Zurita, G., Toto-Arellano, N. I., Meneses-Fabian, C. & Vázquez-Castillo, J. F. "Adjustable lateral-shear single-shot phase-shifting interferometry for moving phase distributions." *Measurement Science and Technology* **20,** 115902 (2009).

39. Strojnik, M., Paez, G. & Mantravadi, M. in *Optical Shop Testing* 122–184 (John Wiley & Sons, Inc., 2006). doi:10.1002/9780470135976.ch4

40. Murty, M. V & hukla, R. P. "Radial shearing interferometers using a laser source." *Applied Optics* **12,** 2765–7 (1973).

41. Matsuda, K., Minami, Y. & Eiju, T. "Novel holographic shearing interferometer for measuring lens lateral aberration." *Applied Optics* **31,** 6603–9 (1992).

42. Ghai, D. P., Vyas, ., enthilkumaran, P. & irohi, R. . "Detection of phase singularity using a lateral shear interferometer." *Optics and Lasers in Engineering* **46,** 419–423 (2008).

43. Patorski, K. " hearing interferometry and the moire method for shear strain determination." *Applied Optics* **27,** 3567–72 (1988).

44. Okoomian, H. J. "A two-beam polarization technique to measure optical phase." *Applied Optics* **8,** 2363_1–2365 (1969).

45. Millerd, J. E., Brock, N. J., Hayes, J. B., North-Morris, M. B., Novak, M. & Wyant, J. . “Pi elated phase-mask dynamic interferometer.” *Proc. SPIE* **5531,** 304–314 (2004).

46. uiro ga, J. A., Antonio G me z-Pedrero, J. & Garc a-Botella, Á. “Algorithm for fringe pattern normalization.” *Optics Communications* **197,** 43–51 (2001).

47. Antonio uiro ga, J. & ervin, M. “ sotropic n-dimensional fringe pattern normalization.” *Optics Communications* **224,** 221–227 (2003).

48. Vest, C. M. "*Holographic Interferometry*". (Wiley Series in Pure & Applied Optics, 1979).

49. Correia, D. P., Ferrao, P. & Caldeira-Pires, A. “Advanced 3D Emission Tomography Flame Temperature ensor.” *Combustion Science and Technology* **163,** 1–24 (2001).

50. Madanipour, K., Fatehi, . & Parvin, P. “Measurement of temperature, refractive index, density distribution, and convective heat transfer coefficient around a vertical wire by the Michelson interferometer.” *Proc. SPIE* **7389,** 73892X–73892X–8 (2009).

51. Aggarwal, A. ., Kaura, . K., hhachhia, D. . & harma, A. . “Holographic optics-based interferometer for real-time testing of phase objects.” *Optics & Laser Technology* **36,** 545–549 (2004).

52. hakher, . & Nirala, A. K. “A review on refractive index and temperature profile measurements using laser-based interferometric techniques.” *Optics and Lasers in Engineering* **31,** 455–491 (1999).

53. Kalal, M. & Nugent, K. A. “Abel inversion using fast Fourier transforms.” *Applied optics* **27,** 1956–1959 (1988).

54. Ampem-Lassen, E., Huntington, S. T., Dragomir, N. M., Nugent, K. A. & Roberts, A. “Refractive inde profiling of a ially symmetric optical fibers: a new technique.” *Optics Express* **13,** 3277–3282 (2005).

55. Zhu, J., Huang, S., Lv, . & Zhou, H. “ tudy on the measurement of temperature field using laser holographic interferometry.” *Frontiers in Energy* **5,** 120–124 (2011).

56. i, J. A., eung, . ., ong, . O. & Probert, . D. “Temperature-field measurements of a premixed butane/air circular impinging-flame using reference-beam interferometry.” *Applied Energy* **83,** 1307–1316 (2006).

57. ervin, M., Estrada, J. . & uiroga, J. A. “The general theory of phase shifting algorithms.” *Optics Express* **17,** 21867–21881 (2009).

58. Dennis C. Ghiglia, M. D. P. "*Two-Dimensional Phase Unwrapping: Theory, Algorithms, and Software*". 512 (Wiley, 1998).

59. Toto-Arellano, N. I., Serrano-García, D. I., Martínez-García, A., Rodríguez-Zurita, G. & Montes-Pérez, A. "4D profile of phase objects through the use of a simultaneous phase shifting quasi-common path interferometer." *Journal of Optics* **115502,** (2011).

60. Vargas, J., uiro ga, J. A., Belenguer, T., ervín, M. & Estrada, J. . "Two-step self-tuning phase-shifting interferometry." *Optics Express* **19,** 638–648 (2011).

61. Vargas, J., uiro ga, J. A., orzano, . O. ., Estrada, J. . & arazo, J. M. "Two-step demodulation based on the Gram– chmidt orthonormalization method." *Optics Letters* **37,** 443 (2012).

62. Otani, Y. in *Handbook of Optical Metrology, Principles and Applications* (Yoshizawa, T.) 615–630 (CRC, 2009).

63. Otani, Y., himada, T., Yoshizawa, T. & me da, N. "Two-dimensional birefringence measurement using the phase shifting technique." *Optical Engineering* **33,** 1604 (1994).

64. in *Polarized Light, Revised and Expanded* (CRC Press, 2003). doi:doi:10.1201/9780203911587.axc

65. Bass, M., tryland, E. . V & illiams, D. R. "Handbook of Optics Volume Classical Optics, Vision Optics, X-Ray Optics 2nd edition." (2001).

66. Onuma, T. & Otani, Y. "A development of two-dimensional birefringence distribution measurement system with a sampling rate of 1.3MHz." *Optics Communications* **315,** 69–73 (2014).

67. "Photonic attice." at <http://www.photonic-lattice.com/>

Published Articles

Journal Articles

1. N. I. Toto-Arellano, D. I. Serrano-García, A. Martínez-García, "Parallel two-step phase shifting interferometry using a double cyclic shear interferometer", *Optics Express*, Vol. 21(26), pp 31983-31989, (2013).
2. D. I. Serrano-García, A. Martínez-García, N. I. Toto-Arellano and Yukitoshi Otani, "Dynamic temperature field measurements using a polarization phase shifting technique", *Optical Engineering*, Vol. 53(11), (2014).
3. D. I. Serrano-García, N. I. Toto-Arellano, A. Martínez-García and G. Rodríguez-Zurita, "Radial slope measurement of dynamic transparent samples", *Journal of Optics***,** Vol. 14, pp 045706-045714, (2012).
4. D. I. Serrano-García, N. I. Toto-Arellano, A. Martínez-García, J. A. Rayas-Álvarez, G. Rodríguez-Zurita and A. Montes-Pérez, "Adjustable-window grating interferometer based on a Mach-Zehnder configuration for phase profile measurements of transparent samples",*Optical Engineering*, Vol. 51, pp 055601-055608, (2012).
5. D. I. Serrano-García, N. I. Toto-Arellano, A. Martínez-García, J. A. Rayas Álvarez and G. Rodríguez-Zurita, "Dynamic phase profile of phase objects based in the use of a quasi-common path interferometer", *Optik*, Vol. 1, pp 1742-1745, (2012).
6. N. I. Toto-Arellano, D. I. Serrano-García, A. Martínez-García, G. Rodríguez-Zurita and A. Montes-Pérez, "4D profile of phase objects through the use of a simultaneous phase shifting quasi-common path interferometer", *Journal of Optics*, Vol. 13, pp 115502-115510, (2011).
7. D. I. Serrano-García, N. I. Toto-Arellano, A. Martínez-García, J. A. Rayas Álvarez, A. Téllez-Quiñones, G. Rodríguez-Zurita, " imultaneous phase-shifting cyclic interferometer for generation of lateral and radial shear", *Revista Mexicana de Física,* Vol. 57(3), pp 0255-0258, (2011).

Book Chapters

1. N. I. Toto-Arellano, D. I. Serrano-García, A. Martínez-García and G. Rodríguez-Zuríta, "Simultaneous Phase Shifting Shearing Interferometry for Measurement of Static and Dynamic Phase Objects", Book: Interferometry - Research and Applications in Science and Technology, Edited by Dr Ivan Padron, ISBN: 978-953-51-0403-2, *InTech*, DOI: 10.5772/34187, (2012).
2. N. I. Toto-Arellano, G. Rodríguez-Zuríta, A. Martínez-García, D. I. Serrano-García and M. G. Hernández-Orduña, "E perimental π Phase-Shifts Observed in the Fourier Spectra of Phase Gratings and Applications in Simultaneous PSI", Book: Interferometry - Research and Applications in Science and Technology, edited by Dr Ivan Padron, ISBN: 978-953-51-0403-2, *InTech*, DOI: 10.5772/36859, (2012).

Technical Handbook

1. N. I. Toto-Arellano, G. Rodríguez Zurita and D. I. Serrano-García, "Teoría Física de Rejillas de Amplitud y Fase", Editorial Académica Española, ISBN-10: 384657030, (2011).

Conference Proceedings

1. D. I. Serrano-García, A. Martínez-García, J. A. Rayas-Álvarez, G. Rodríguez-Zuríta and A. Montes-Pérez, "Parallel phase shifting interferometry using a double cyclic shear interferometer", N. I. Toto-Arellano, 22nd Congress of the International Commission for Optics: Light for the Development of the World, Proceedings of the SPIE, Volume 8011, article id. 80110N, 6 pp. (2011).
2. D. I. Serrano-García, N. I. Toto-Arellano, A. Martínez-García, J. A. Rayas-Álvarez and G. Rodríguez-Zuríta, "Simultaneous phase shifting interferometry based in a Mach Zehnder interferometer for measurement of transparent samples", 22nd Congress of the International Commission for Optics: Light for the Development of the World, Proceedings of the SPIE, Volume 8011, article id. 80110M, 6 pp. (2011).

3. N. I. Toto-Arellano, A. Martínez-García, J. A. Rayas-Álvarez, D. I. Serrano-García, "Slope measurement of a phase object", 22nd Congress of the International Commission for Optics: Light for the Development of the World, Proceedings of the SPIE, Volume 8011, article id. 80110P, 6 pp. (2011).
4. D. I. Serrano-García, N. I. Toto-Arellano, A. Martínez-García and G. Rodríguez-Zurita, "Radial slope measurements of transparent samples using phase shifting interferometry by polarization", Eighth Symposium Optics in Industry, Proceedings of SPIE Volume 8287, article id. 828714, 6 pp. (2011).
5. D. I. Serrano-García, N. I. Toto-Arellano, A. Martínez-García, G. Rodríguez-Zurita and A. Montes-Pérez, "Single shot phase shifting interferometry for measurement of transparent samples", Dimensional Optical Metrology and Inspection for Practical Applications, Proceedings of SPIE Volume 8133, article id. 8133 0X, 6 pp. (2011).

Awards Received

1. Best Student Presentation Award granted by OSA during 2013 CIOMP-OSA Summer Session: Optical Engineering, Design and Manufacturing. Changchun, China, August 2013.
2. Scholarship granted by SPIE, the International Society for Optics and Photonics for his potential contributions to the field of optics, photonics or related field. San Diego, Californía, USA, August 2011.
3. Full Travel Grant granted by the APS to assist the 5th Canadian-American-Mexican Graduate Student Physics Conference. Washington D.C, USA, September 2011.
4. OSA Foundation travel grant to assist The Frontiers in Optics 2011 Conference.San Jose, California, USA, October 2011.
5. 1st Place SPIE Student Poster Presentation during the 22nd International Commission for Optics (ICO-22). Puebla, Puebla, México. August 2011.